Numerical study of hydrogen influence on void growth at low triaxialities considering transient effects

A. Díaz , J.M. Alegre , I.I. Cuesta , Z. Zhang

PII: S0020-7403(19)31992-7
DOI: https://doi.org/10.1016/j.ijmecsci.2019.105176
Reference: MS 105176

To appear in: *International Journal of Mechanical Sciences*

Received date: 3 June 2019
Revised date: 30 July 2019
Accepted date: 18 September 2019

Please cite this article as: A. Díaz , J.M. Alegre , I.I. Cuesta , Z. Zhang , Numerical study of hydrogen influence on void growth at low triaxialities considering transient effects, *International Journal of Mechanical Sciences* (2019), doi: https://doi.org/10.1016/j.ijmecsci.2019.105176

Highlights:

- Hydrogen redistribution around a void is analysed considering transient effects.
- Coupled diffusion, trapping effects and local softening are implemented in ABAQUS.
- Unit cell analysis shows necking failure without hydrogen at low triaxialities.
- Hydrogen depletion due to the creation of traps occurs at high strain rates.
- Hydrogen redistribution and local softening determine the shear band formation.

Numerical study of hydrogen influence on void growth at low triaxialities considering transient effects

A. Díaz[1*], J. M. Alegre[1], I. I. Cuesta[1], Z. Zhang[2]

[1]Structural Integrity Group, Universidad de Burgos, Escuela Politécnica Superior. Av Cantabria s/n, 09006 Burgos, Spain

[2]NTNU Nanomechanical lab, Department of Structural Engineering, Norwegian University of Science and Technology (NTNU), Trondheim, 7491, Norway

*Corresponding author: adportugal@ubu.es +34 947258923

Abstract

Assuming that hydrogen enhances localised plasticity, as one of the leading mechanisms proposed in the literature, the void growth and coalescence are modified by local softening and ductile failure features depend on hydrogen accumulation. It is anticipated that strain rate plays an important role in hydrogen-informed void mechanisms, however, coupling voids, transient hydrogen diffusion, rate-dependent hydrogen-material interactions and intrinsic hardening, remains a challenge. In this study, the simulation of a void unit cell in a hydrogen pre-charged material is reconsidered here for the first time to incorporate transient effects, i.e. the kinetic redistribution of hydrogen around a void subjected to a high strain rate and a constant stress triaxiality. A coupled diffusion-mechanics scheme is implemented in a set of ABAQUS subroutines in order to analyse the interaction of hydrogen with the material response. The influence of strain rate is also considered when defining the cell boundary conditions through the limiting cases of equilibrium and insulated unit cells. The competition between the two inherent mechanisms, namely, hydrogen softening and strain rate hardening, is studied with the implemented framework. Results show that transient effects determine hydrogen concentrations and strongly dictate failure mechanisms: shearing might occur due to the hydrogen induced softening for moderate strain rates even though the cell is insulated. However, for very fast loading it is demonstrated that the fast creation of traps due to plastic deformation results in hydrogen depletion and necking failure is observed.

Keywords: Hydrogen embrittlement, Hydrogen diffusion, Void Growth, Unit Cell Simulations

1. Introduction

One of the proposed mechanisms to explain hydrogen embrittlement phenomena is the so-called HELP (hydrogen enhanced localised plasticity) [1,2]. Hydrogen increases dislocation mobility and slip localisation. Thus, a local softening is produced, and this can lead to strain localization. Although the fracture might seem brittle in the macroscale, actually there is a localised plasticity [3]. Recently, Martin et al. reviewed experimental and numerical evidences of HELP as a viable embrittlement mechanism for a wide range of alloys [4]. Therefore, the void nucleation, growth, and coalescence are affected by the inserted hydrogen. The competition between localised plasticity and decohesion near a crack tip in high-triaxiality regions has been a matter

of debate during the last decades among hydrogen embrittlement researchers [5]. However, the aim of this study is to analyse hydrogen effects in the void growth, i.e. in the second stage of ductile failure, so decohesion is not considered here.

Experimentally, some authors have observed a change in failure mode due to hydrogen. Matsuo et al. [6] found that hydrogen reduced the ductility during a tensile test; however, as illustrated in Figure 1, the apparent embrittlement is due to a change in void growth and coalescence: when hydrogen is absent, voids are elongated and the final failure is due to necking whereas hydrogen promotes shearing. This fact was explained by the authors because hydrogen enhances localised slip deformation.

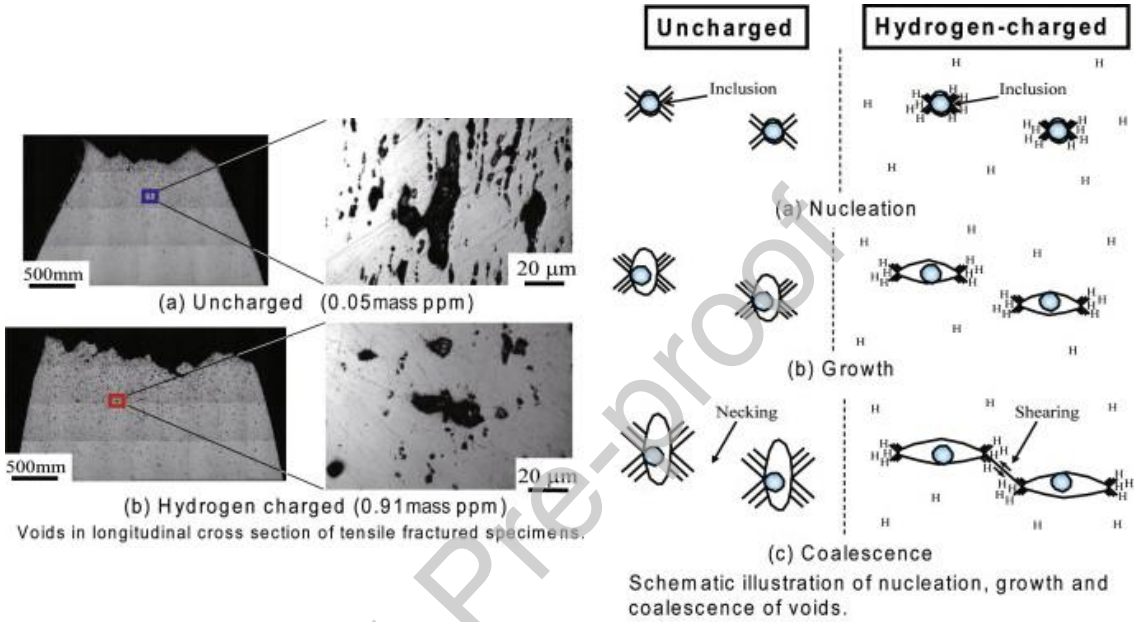

Figure 1. Comparison between the hydrogen-enhanced shearing and the void necking in the absence of hydrogen. Experimental results in a tensile test and proposed micro-mechanisms (extracted from [7])

Considering that at low triaxialities, e.g. in tensile tests, ductile fracture is predominant even at high hydrogen concentrations, the interaction of hydrogen with voids should be better understood. Even though some authors have already dealt with the simulation of void growth and coalescence in the presence of hydrogen, numerical modelling at the microscale has focused on the behaviour of hydrogen near a crack tip due to the fact that hydrogen effects are more pronounced at high triaxialities [8–11] .

Different approaches might be considered to model ductile fracture in metals. Porosity based continuum models, e.g. the Gurson model and its subsequent modifications, have achieved great success in the prediction of this kind of failures [12]. Nevertheless, some parameters involved are hardly linked with physical behaviour. Another computational approach is based on the simulation of unit cells with a central spheroidal void [13]. Nucleation of voids is difficult to simulate so most of the research has focused on growth and coalescence stages.

Sofronis et al. [3], as the proposers of HELP theory, have tried to evaluate numerically the macroscopic effects of a local softening due to hydrogen. Ahn et al. [14] have established a consistent strategy to implement an informed cohesive model in which Traction Separation Laws (TSL) are based on the behaviour of a void unit cell within a hydrogen environment producing local softening. Within that framework, Yu et al. [15] modified the softening law in

order to consider a more realistic shearing failure induced by hydrogen and obtained a failure loci for different triaxialities.

In the aforementioned numerical studies, only quasi-static situations were considered. In those conditions, unit cells dimensions are trivial, and hydrogen distribution is assumed to follow thermodynamic equilibrium. From this perspective, hydrogen concentrations are univocally obtained by the stress state and only a steady state analysis is performed. As will be discussed, if transient and kinetic effects are taken into account, a new characteristic length is introduced, and the problem becomes size dependent.

Another aspect that might be considered when evaluating a characteristic length is the use of non-local models or strain gradient theories. The Strain Gradient Plasticity (SGP) theories predict higher stress near a crack tip [16,17] and thus higher hydrogen concentrations [11]. Additionally, SGP influences void growth and coalescence [18]. Horstemeyer et al. have studied the coupling of length and time scales in plasticity from an atomistic point of view [18]. However, the restriction of time and size in MD simulations limits a bottom-up understanding of length scales. From a continuum point of view, Fokoua et al. [19] show a competition between instabilities due to strain localization and regularization introduced by non-local plasticity. This can be used to scale plasticity behaviour and to understand better ductile failure due to void growth and coalescence. However, the present paper does not consider these size – influenced models.

In order to validate the quasi-static, size-independent approach, it should be discussed for each particular situation whether diffusion is so fast that hydrogen concentration instantaneously follows the stress-state or not. It has been shown that strain rate highly affects, as it happens with most of the environmental degradation phenomena, hydrogen embrittlement [20]. Hydrogen-enhanced fatigue crack growth has been demonstrated to critically depend on load frequency [21,22]. This suggests a need for a transient analysis. In addition, when traps are considered, the creation of dislocations and plastic strain rate are crucial variables in hydrogen transport modelling [10]. The redistribution of hydrogen around a void is thus time dependent and a transient analysis must be considered and compared with the steady state case. This time dependency is related to a length scale by means of the diffusivity.

Many experimental studies have shown that susceptibility to hydrogen embrittlement is reduced at high strain rates since there is not enough time for hydrogen to diffuse to the Fracture Process Zone (FPZ) [23]. These results have been found both in tensile [24] and in fracture tests [25]. In these cases, a diffusion length might be defined and compared to the distance to the fracture initiation location [22].

Even, in precharged specimens, where diffusion from the external source is not critical, hydrogen accumulation in the high hydrostatic regions will depend on the length scales associated with hydrogen transport. Once it is assumed that hydrogen is accumulated in highly stressed regions, another length scale might be defined by considering the transient redistribution of hydrogen around a void during its growth. Transient redistribution is a phenomenon coupled with local hydrogen softening and strain localization which can govern the mode of failure. In the present paper, the analogy between heat transfer and hydrogen diffusion is exploited in order to study strain localization.

When the ductile failure is triggered by a rapid load, hydrogen is not able to accumulate in the FPZ. However, precharged hydrogen is redistributed near the void even at high strain rates. In this case, the Representative Volume Element, i.e. the unit cell, might be regarded as insulated.

This situation is similar to the adiabatic shear instabilities due to thermal softening [26]: for high strain rates dissipation is not possible and thermal softening overcomes strain and strain rate hardening phenomena. The development of shear banding was simulated in void unit cells by Zhu and Batra [27]. In a similar way, for high strain rates in hydrogen environments, there is no time for hydrogen to accumulate in the FPZ -since the cell is "insulated" due to the rapid load- but then, kinetic effects should be taken into account. Two questions are posed here: (i) Is it possible that less hydrogen –due to insulated conditions– could be more concentrated in dislocations during fast loads and produce higher instabilities? (ii) Since slow strain rates imply a thermodynamic equilibrium for hydrogen concentrations, does the transient approach lack its usefulness? On the other hand, for very rapid loads, even at low triaxialities, cleavage fracture might predominate, so, is it meaningful to simulate very high strain rates within a void unit cell model? The present paper tries to understand these two questions by reproducing different conditions – insulated versus equilibrium situations – and different values of strain rates.

Hydrogen initial concentration and triaxiality are two values extracted from a "global model" in the FPZ. Hence, it is analysed here a local redistribution and the interactions between hydrogen accumulation and strain localization near a void. Hydrogen exchange between adjacent cells is neglected here, but in future research boundary conditions should capture the hydrogen transport during the loading process, extracting these conditions from a global diffusion model.

The objective of this study is to assess the influence of different hydrogen-related parameters on the void growth leading to ductile failure. FEM results might indicate the mode of failure of the void -necking or shear banding- but the discussion about a coalescence criterion is out of the scope of the present paper. Additionally, due to the importance of transient effects, a possible rate-dependent material is considered.

The paper is organized as follows. Equations governing hydrogen diffusion are presented in Section 2. After the proposition of possible transient effects, the emphasis is put on length scales, derived from the diffusion model previously described, and the analogy between hydrogen diffusion and heat transfer is discussed. Hardening laws are given in Section 3, with a short exposition of the HELP mechanism and the related softening parameters. With the aim of analysing those transient effects, Finite Element implementation of the coupled problem is described in Section 4. Simulations reproducing a void, initially spherical, in an axisymmetric unit cell are defined. Section 5 presents and discussed the results of these simulations and, finally, conclusions are summarised in Section 6.

2. Hydrogen diffusion modelling

2.1. Equations governing hydrogen diffusion

A two-level model is chosen to model hydrogen diffusion in which two species of hydrogen are included in the mass balance: interstitial and trapped hydrogen. L subscript refers to hydrogen located in lattice sites while T subscript corresponds to hydrogen in trapping sites [9]. Hydrogen flux throughout the lattice is assumed to follow the Fick's first law, modified by a hydrostatic stress term that takes into account the chemical potential reduction in tensile regions [28]. An additional term is included, following Krom et al. [10] to consider the influence of trap creation during plastic straining. The mass balance finally might be expressed as a single equation:

$$N_T \frac{\partial \theta_T}{\partial t} + \frac{\partial C_L}{\partial t} - \nabla \cdot (D_L \nabla C_L) + \nabla \cdot \left(\frac{C_L D_L \bar{V}_H}{RT} \nabla \sigma_h \right) + \theta_T \frac{dN_T}{d\varepsilon^p} \frac{\partial \varepsilon^p}{\partial t} = 0 \#(1)$$

where C_L is the concentration in lattice sites, D_L the ideal diffusivity, $\bar{V}_H$ the partial molar volume of hydrogen, σ_h the hydrostatic stress, T the temperature and R the ideal gas constant. The density of trapping sites N_T depends on equivalent plastic strain ε^p because of the creation of dislocations acting as retention sites for hydrogen [29]:

$$\log N_T = 23.26 - 2.33 \exp(-5.5\varepsilon^p) \#(2)$$

Krom et al. [10] demonstrated that if the last term in (2) is not included, hydrogen is created in insulated conditions, which violates the mass balance. Besides C_L, occupancy of traps θ_T is the second dependent variable of the partial differential equation expressed in (1). An additional equation is needed, which usually is derived from thermodynamic equilibrium firstly proposed by Oriani [30]. However, due to the transient nature of this study, it is necessary to include the kinetic formulation firstly proposed by McNabb and Foster [31]:

$$\frac{\partial \theta_T}{\partial t} = p\frac{C_L}{N_L}(1-\theta_T) - k\theta_T \#(3)$$

where N_L is the density of lattice sites; k and p are the trapping and detrapping frequencies, respectively [32]. Both constants are assumed to follow an Arrhenius law with trapping and detrapping energies, E_t and E_d, and considering the same hop attempt frequency, ν.

$$k = \nu \exp\left(-\frac{E_t}{RT}\right) \#(4)$$

$$p = \nu \exp\left(-\frac{E_d}{RT}\right) \#(5)$$

The difference between E_d and E_t is usually expressed as a binding energy: $E_B = E_d - E_t$. This value characterises the trapping intensity of defects. Empirically, Thermal Desorption Spectroscopy, also called Thermal Desorption Analysis, (TDS or TDA) is the most used technique to evaluate detrapping or binding energies.

2.2. Analogy with heat transfer

Three physical processes are often included in the "transport phenomena" category since they are governed by similar equations: diffusion, heat transfer and momentum balance [33]. This is not only useful for didactic purposes, but it reduces notably the efforts to find a possible analytical solution and simplifies the numerical implementation. For instance, many FEM commercial codes include sophisticated heat transfer modules whereas mass transfer analysis is more limited. This is why some authors have proposed to exploit the analogy between heat transfer and mass diffusion in order to implement complex hydrogen transport models [34–36].

Fick's first law is analogous to the Fourier's law, hence an equivalence between diffusivity and conductivity might be established. Similarly, a mass balance, i.e. the Fick's second law, might be associated with the energy balance in a heat transfer analysis.

The analogy with the heat transfer problem might be extended for the hydrogen transport model including trapping effects and a hydrostatic stress term. Krom's term [10], which includes the influence of the plastic strain rate of trap creation, could be regarded as an internal source or sink of hydrogen. In the same way, an internal source of energy is the plastic dissipation in an energy balance equation. Following Gurtin's thermodynamic approach [37]:

$$\rho c_p \frac{\partial T}{\partial t} - \nabla \cdot (k\,\nabla T) + \underbrace{(2\mu + 3\lambda)\alpha\ \mathrm{tr}\,\dot{\mathbf{E}}^e}_{Thermal\ expansion} - \underbrace{Y_{dis}(\varepsilon^p, T)\frac{\partial \varepsilon^p}{\partial t}}_{Plastic\ dissipation} = 0 \#(6)$$

Where μ and λ are the Lame moduli, α is the thermal expansion coefficient, tr $\dot{\mathbf{E}}^e$ is the trace of the elastic strain rate tensor, $Y_{dis}(\varepsilon^p, T)$ is the dissipative part of the flow resistance. The relationship between the trace of volumetric elastic strain tr $\mathbf{E}^e$ and the hydrostatic stress is established through the bulk modulus:

$$\sigma_h = 3K \text{ tr } \mathbf{E}^e \#(7)$$

Diffusion equation for the two-level modelling is similar, but here the hydrostatic stress term emerges from the enhanced diffusion towards regions with high hydrostatic stress and not from the hydrogen-induced dilatation. Di Leo et al. [38] propose a governing equation for the chemical potential rather than a mass balance for C_L. In that case, the expansion term includes tr $\dot{\mathbf{E}}^e$ and avoids the gradient calculation of hydrostatic stress. However, following the classic approach of Sofronis & McMeeking [9], the term included in equation (1) is implemented. The dissipative term introduces a strain rate influence.

Heat transfer	**Hydrogen diffusion**
T	C_L
k	D_L
ρc_p	D_L/D_{eff}
$(2\mu + 3\lambda)\alpha$ tr $\dot{\mathbf{E}}^e$	$\nabla \cdot \left(\frac{C_L D_L \bar{V}_H}{RT} \nabla \sigma_h \right)$
$Y_{dis}(\varepsilon^p, T)$	$\theta_T \frac{dN_T}{d\varepsilon^p}$

Table 1. Analogy between heat transfer and hydrogen transport governing variables and terms.

2.3. Definition of length scales

A diffusion distance might be defined as [22]:

$$x \propto \sqrt{Dt} \#(8)$$

where x is the mean distance that a hydrogen atom would have diffused in a time t; the equation (8) is related with random walk and was firstly derived for the explanation of Brownian motion [39] and the relationship of proportionality might be substituted by an equality by introducing a geometric constant: $x = \gamma\sqrt{Dt}$. Diffusivity D can be derived from a statistical mechanics approach [40]. However, within a continuum framework, crystal defects such as dislocations, vacancies, grain boundaries, etc, could act as trapping sites delaying hydrogen diffusion. In this case, an effective diffusivity will be defined D_{eff}. Delaying implies that $D_{eff} < D_L$, being D_L the diffusivity in the perfect crystal [41].

Effective diffusivity not only depends on material features; it also depends on the hydrogen concentration, so the length scale of diffusion is not known a priori, but it depends on the numerical solution.

$$x_{diff} \propto \sqrt{D_{eff}\, t} \#(9)$$

Wu et al. [42] for thermal softening define a characteristic length associated with thermal diffusion over the time interval t.

$$x_{diff} \propto \sqrt{\frac{kt}{\rho c_p}} \#(10)$$

This expression allows establishing a simple criterion to differentiate between adiabatic, non-thermal and the intermediate situation. Comparing the energy balance equation in the heat transfer problem with the mass balance in the hydrogen diffusion problem, the equivalences shown in Table 1 are found for the length scale definition: $D_L/D_{eff} \equiv \rho c_p$ and $D_L \equiv k$. Therefore, hydrogen redistribution in a unit cell can also be classified in two limiting cases: insulated or equilibrium conditions, depending on the diffusion length associated with material properties, i.e. with effective diffusivity, and with the elapsed time. In the present work, transient effects will be discussed as a function of the equivalent strain rate, $\dot{E}_e$; this mesoscopic strain is defined in Section 4 for a unit cell analysis and must not be confused with the strain rate tensor $\dot{\mathbf{E}}^e$. Thus, the diffusion length might be expressed as:

$$x_{diff} = \sqrt{\frac{D_{eff}}{\dot{E}_e}} \#(11)$$

Assuming thermodynamic equilibrium, and for low lattice concentrations $C_L \ll N_L$, Sofronis and McMeeking [9] defined an effective diffusivity:

$$D_{eff} = \frac{D_L}{1 + \frac{C_T}{C_L}(1 - \theta_T)} \#(12)$$

It must be noted here that the strain rate is a mesoscopic parameter, i.e. defined for the void unit cell, whereas the effective diffusivity depends on local magnitudes like hydrogen concentration and the density of traps. Therefore, traps might be considered as beneficial for mitigating hydrogen embrittlement at certain strain rates. This fact has been demonstrated experimentally, as in [22] for vanadium carbides acting as strong traps, and has been numerically modelled [43]. The ratio between diffusion length and the unit cell dimensions will determine the nature of hydrogen redistribution:

$$\begin{array}{lll} x_{diff} \ll R_0 & \rightarrow & \text{Insulated conditions} \\ x_{diff} \gg R_0 & \rightarrow & \text{Equilibrium conditions} \end{array} \#$$

where R_0 is the initial cell radius. Considering again the thermal analogy, these extreme cases might be linked to the adiabatic and non-thermal situations, respectively [42]. Intermediate cases are not analysed here since more complex boundary conditions must be considered.

3. Local hardening and softening

It is extremely difficult to separate all contributions from temperature, plastic strain and strain rate in the hardening/softening behaviour which can lead to the strain localization and thus to the shear banding or necking modes of failure. Even more, if hydrogen effects are included in hardening law, the problem becomes very complex. Hardening law h is considered as a function of the involved parameters:

$$\sigma_Y = \sigma_0\, h\left(\varepsilon^p, c_H, \dot{\varepsilon^p}, T\right) \#(13)$$

where σ_0 is the initial yield stress, ε^p is the equivalent plastic strain, $\dot{\varepsilon^p}$ the equivalent plastic strain rate, c_H a normalised hydrogen local concentration and T the temperature. Each contribution is assumed to operate independently through individual hardening expressions h_i:

$$\sigma_Y = \sigma_0\, h_1(\varepsilon^p) h_2(c_H) h_3\left(\dot{\varepsilon^p}\right) h_4(T) \#(14)$$

where h_1, h_2, h_3 and h_4 are the softening/hardening induced by equivalent plastic strain, by hydrogen, by equivalent plastic strain rate and by temperature, respectively. For the sake of simplicity, thermal softening is neglected here so $h_4(T)$ = 1. Nonetheless, it should be noted that even in the absence of external sources of heat, plastic deformation might induce a significant local raise of temperature, leading to the thermal softening phenomenon.

Work hardening is assumed to follow a power law with a strain hardening exponent n.

$$h_1(\varepsilon^p) = \left(1 + E\frac{\varepsilon^p}{\sigma_0}\right)^n \#(15)$$

where E is the Young's modulus and n is the hardening exponent. The influence of hydrogen on the plastic behaviour of metals is still not well understood. However, the interaction of hydrogen with dislocations seems to trigger a local softening. Sofronis and coworkers [3] proposed a simple lineal softening law:

$$h_2(c_H) = \begin{cases} (\xi - 1)c_H + 1, & h_2(c_H) > \zeta \\ \zeta, & h_2(c_H) \leq \zeta \end{cases} \#(16)$$

where ξ is an indicator of hydrogen softening and ζ represents the stress limit that cannot be reduced even at extremely high concentrations. For example, ζ = 0.5, initial yield stress σ_0 might be reduced only to the 50 % in the presence of hydrogen. Yu et al. [15] argued that a linear softening could not lead to a shearing failure and they replaced it with a sigmoidal softening law.

$$h_2(c_H) = 1 + \frac{\zeta - 1}{1 + \exp\left[-k\left(c_H - c_{H,0}\right)\right]} \#(17)$$

where the total hydrogen concentration has been normalised $c_H = (C_L + C_T)/C_0^S$. The authors [15] considered $c_{H,0}$ = 1.15 and ζ = 0.5 and evaluated the influence of k value. Those values are based on the observations from Zhang et al. results [44]. The concentration level at which hydrogen softening begins is represented by C_0^S. In the present paper, it is assumed, that C_0^S equals the initial lattice concentration; however, this assumption will be discussed later. Figure 2 compares the softening laws that are considered in the simulations presented in Section 5.

However, the physical implications of these phenomenological laws and the value of softening parameters ξ, ζ and k must be still clarified. Atomistic simulations [45,46] or discrete dislocation dynamics (DDD) [47,48] approaches could shed light on the complex interaction between plastic phenomena and hydrogen local concentrations. That discussion is out of the scope of the present work.

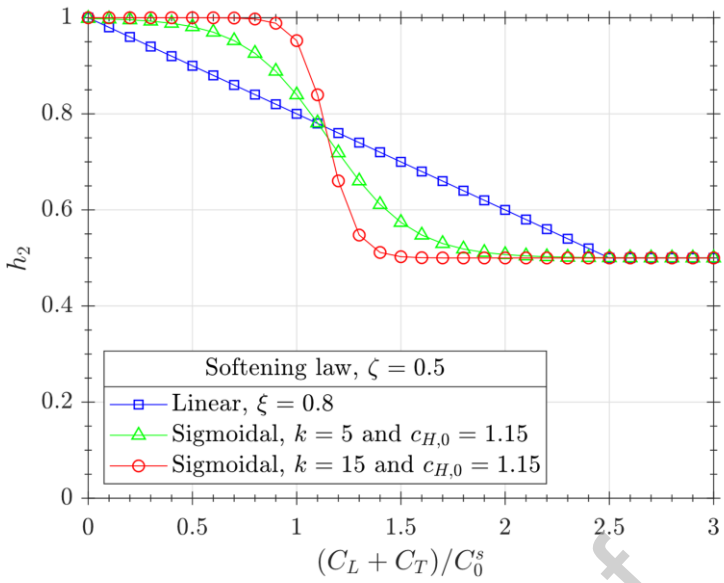

Figure 2. Comparison between a linear softening law proposed by Sofronis et al. [3] and a sigmoidal softening law proposed by Yu et al. [15].

Finally, in order to analyse realistically the void behaviour during fast loads, a rate dependent material is consid

$$h_3(\dot{\varepsilon^p}) = \left[\frac{\dot{\varepsilon^p}}{\dot{\varepsilon_0^p}}\right]^m \quad \#(18)$$

Strain rate has a double effect: on one hand, strain rate hardening might be important for high strain rates and, on the other hand, plastic strain rate could affect kinetics of trapping. When $\dot{\varepsilon^p}$ is high, dislocations are multiplied very fast. The rapid creations of those traps promote the depletion of interstitials in these regions [10]. All these softening effects and their relationship with the abovementioned coupled mechanisms between diffusion and the stress-strain state are presented in Figure 3.

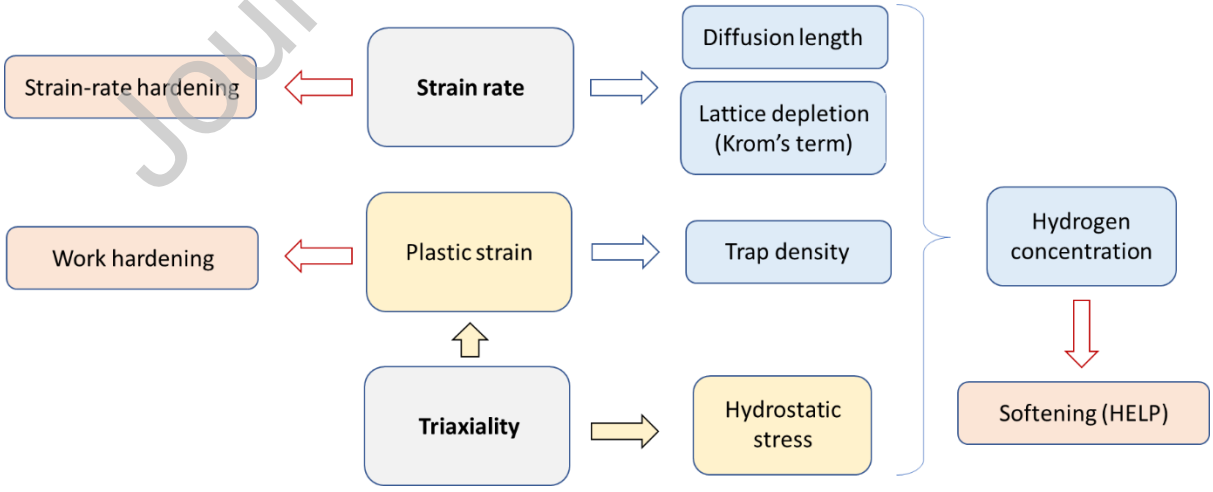

Figure 3. Map of the coupled phenomena. Strain rate and triaxiality are the loading inputs (in grey) producing the local stress-strain response (in yellow).

Plastic strain and hydrostatic stress promote hydrogen accumulation on trapping and lattice sites, respectively. In addition, if transient effects are considered, a diffusion length might be

defined and Krom's term suggests a lattice depletion at high strain rates. A coupled competition is then established between strain-rate and work hardening against local softening enhanced by hydrogen. These three mechanisms, in combination with triaxiality, will determine the void growth and the possible apparition of shearing.

4. Void Unit Cell Simulations

4.1. Cell modelling

A Representative Volume Element is simulated considering a spherical void in an axisymmetric unit cell. This approach has been followed by many authors with the aim of evaluating void growth and mesoscopic stress-strain response of a unit cell subjected to a load and assessing triaxiality influence [49], strain hardening [50], prestrain history [51],the effect of initial porosity [52], the effect of initial void shape [53], material length scale in SGP [54], etc. The bulk material is assumed to have a uniform population of voids with a separation between adjacent voids of $2R_0$ horizontally and $2H_0$ vertically; the hexagonal prism is then simplified as a cylinder in order to model an axisymmetric cell, as shown in Figure 4.

During loading, the external faces of the unit cell are forced to remain perpendicular so the main dimensions of the unit cell H and R are computed following the expressions:

$$H = H_0 + U_z \#(19)$$

$$R = R_0 + U_r \#(20)$$

where U_z is the axial displacement of the upper face and U_r the radial displacement of the outer cylinder surface. When size effects are not taken into account, unit cell dimensions are not important and only the ratio between void and unit cell sizes is related to porosity.

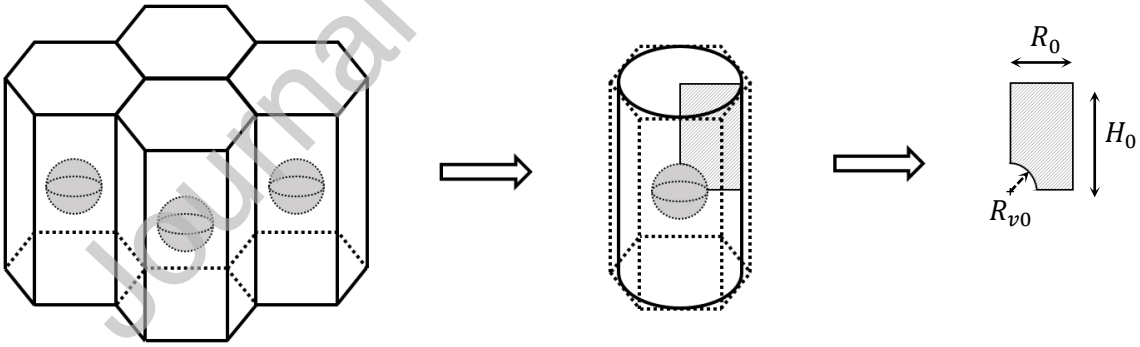

Figure 4. Axisymmetric model representing a void unit cell. Hexagonal prisms RVE are simplified as cylinders [55].

The effect of prolate or oblate voids is not analysed here so the void is initially spherical, $H_0 = R_0$, and initial porosity might be calculated [53]:

$$f_0 = \frac{2}{3}\left(\frac{R_{v0}}{R_0}\right)^3 \#(21)$$

Here, unit cell dimensions have been simulated as: $H_0 = R_0 = 0.04$ mm, whereas $R_{v0} = H_{v0} =$ 0.005 mm, giving an initial porosity of $f_0 = 0.0013$ and $W_0 = 1$. Even though voids are spherical in the initial geometry, the void shape change $W = H_v/R_v$ is registered during loading in order

to analyse triaxiality and hydrogen effects; for low triaxialities, the void is axially elongated so a shape $W > 1$ is expected whereas for high triaxialities $W < 1$ should be found. The mesh is shown in Figure 5. It consists of 3000 quadratic quadrilateral elements of type CAX8RT with 9222 nodes. This mesh has been chosen following the mesh sensitivity analysis performed by Yu et al. [15]; the authors demonstrated that this mesh captures shear banding accurately.

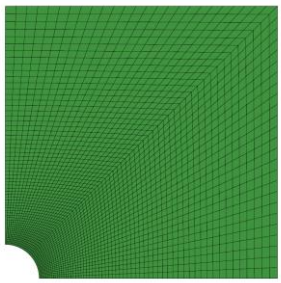

Figure 5. Mesh of the axisymmetric model.

RVE simulations might be performed by applying mesoscopic loads at the top and lateral surfaces, Σ_r and Σ_z respectively or by a displacement-controlled loading with U_r and U_z. The procedure followed here, as explained in the next subsection, is based on the selection of a U_z ramp and the calculation of the corresponding U_r that keeps a constant triaxiality. In order to analyse the stress-strain curve of the void unit cell, it is useful to define an equivalent stress and strain:

$$\Sigma_e = |\Sigma_z - \Sigma_r| \#(22)$$

$$E_e = \frac{2}{3}|E_z - E_r| \#(23)$$

where the axial and radial mesoscopic strains depend on the displacement of the cell faces whose values are registered in the corner node of the axisymmetric model.

$$E_r = \ln\left(\frac{R}{R_0}\right) = \ln\left(1 + \frac{U_r}{R_0}\right) \#(24)$$

$$E_z = \ln\left(\frac{H}{H_0}\right) = \ln\left(1 + \frac{U_z}{H_0}\right) \#(25)$$

Additionally, a mesoscopic mean stress Σ_m might be defined and then triaxiality η can be expressed as a function of the biaxial stress ratio $\rho = \Sigma_r/\Sigma_z$

$$\Sigma_m = \frac{1}{3}(\Sigma_z + 2\Sigma_r) \#(26)$$

$$\eta = \frac{\Sigma_m}{\Sigma_e} = \frac{1}{3}\frac{1+2\rho}{|1-\rho|} \#(27)$$

The results presented in Section 5 are focused on low triaxialities (η = 0.7) even though higher stress ratios are also analysed.

4.2. Boundary and initial conditions for diffusion

Considering that a phenomenon similar to adiabatic shear banding is expected here, the unit cell must be considered as insulated since the strain rate is high enough to disregard mass exchange between adjacent cells. A zero-flux boundary condition is thus taken into account.

There will be a non-zero flux through the void surface and a consequent build-up of internal pressure up to an equilibrium pressure, but here, this physical phenomenon is neglected, and the void surface is assumed as insulated.

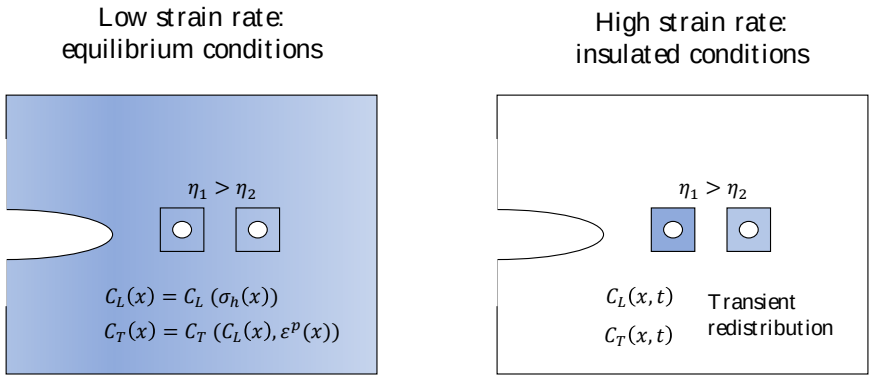

Figure 6. Equilibrium vs. insulated conditions. In the first case, hydrogen concentration around the void is determined by the stress-strain state. However, when the load is fast, material points might be regarded as insulated and hydrogen only has enough time to redistribute locally.

The initial conditions for the Partial Differential Equation (1) are established considering a uniform hydrogen concentration in lattice sites C_{L0} and the corresponding concentration in trapping sites assuming thermodynamic equilibrium [56]:

$$C_L(x, t = 0) = C_{L0} \#(28)$$

$$C_T(x, t = 0) = \frac{N_{T,0}}{1 + \dfrac{N_L}{C_{L,0} \exp\left(\dfrac{E_b}{RT}\right)}} \#(29)$$

From these initial conditions, hydrogen accumulation within a kinetic framework will deviate from the thermodynamic equilibrium depending on the length scale, i.e. on the strain rate.

4.3. Numerical implementation

Hydrogen diffusion equations, shown in section 2, are implemented by means of a UMATHT subroutine in which the heat transfer analogy is exploited: a flux and internal thermal energy must be defined [35]. The implementation of McNabb and Foster equations is usually problematic due to convergence issues and numerical instabilities. Implementation of the two PDE (1) and (3) might lead to numerical instabilities, especially at high values of vibration frequencies. In the present work, the numerical implementation follows the analytical approximation proposed by Benannoune et al. [57]. The occupancy of traps is calculated as:

$$\theta_T = \left(\theta_T^0 - \frac{p\theta_L}{p\theta_L + k}\right) \exp[-(p\theta_L + k)t] + \frac{p\theta_L}{p\theta_L + k} \#(30)$$

where θ_T^0 is the hydrogen occupancy of traps at t = 0.

Using the UMATHT approach, the temperature degree of freedom is occupied by concentration, thus some thermal effects on diffusion cannot be considered, as Soret effect or heat sources due to plastic straining. Writing a UEL might solve this problem; Di Leo et al. [38] consider this strategy but they do not simulate thermal effects.

An algorithm to keep triaxiality constant is also required; in that case, an MPC subroutine is used [58]. Since the plastic instabilities would affect the mesoscopic stresses and strains, it is not possible to fix a priori the equivalent strain rate $\dot{E}_e$ for the unit cell. Therefore, in FEM simulations an axial displacement rate is fixed: $\dot{U}_z = \Delta U_z / t_{load}$ whereas the radial displacement U_r is calculated by the MPC subroutine to keep a constant triaxiality; at each increment the evolution of E_e is also registered. Hence the effect comparison of different softening parameters is not straightforward.

The material parameters that have been used in the simulations presented in Section 5 are summarised in Tables 2 and 3. Most of these values are extracted from the pioneering work on diffusion modelling of Sofronis and McMeeking [9]. The unit cell dimensions and the softening-related parameters are extracted from [15].

$H_0 = R_0$ [mm]	0.04
f_0 [–]	0.0013
$\dot{U}_z$ [mm·s^{-1}]	10^{-3}(equilibrium) 1.0; 10; 100 (insulated)
η [–]	0.7

Table 2. Parameters for unit cell simulations.

E [MPa]	210000	D_L [mm^2·s^{-1}]	0.0127
ν [–]	0.3	$C_{L,0} = C_0^s$ [wt ppm]	10^{-3}; 1.0
σ_0 [MPa]	400	N_L [sites·m^{-3}]	5.1×10^{29}
n [–]	0.1	N_T [sites·m^{-3}]	Eq. (2)
ζ [–]	0.5	$\bar{V}_H$ [mm^{3}mol^{-1}]	2000
ξ [–]	0.8	E_b [kJ·mol^{-1}]	30; 40; 50
k [–]	5; 15	T [K]	300
$\dot{\varepsilon}_0^p$ [s^{-1}]	0.001	E_t [kJ·mol^{-1}]	12.9
m [–]	0; 0.05; 0.10	ν [s^{-1}]	10^{13}

Table 3. Parameters governing elastic-plastic behaviour and for hydrogen transport modelling.

5. Results

The objective of this paper is to evaluate void growth so void volume fraction f is registered during the unit cell loading. Three approaches are possible: (i) to assume incompressibility and

consider that the cell volume increment is only caused by the void growth; (ii) to register the evolution of void radii $R_v(t)$ and $H_v(t)$ and assume that the void shape might be approximated to an ellipsoid, which is inaccurate for low triaxialities because the void surface is very abrupt for same stages of loading; and (iii) to calculate void volume by integrating the void surface coordinates following the disk method for a solid of revolution:

$$V_{void}(E_e) = 2\pi \int_0^{z=H_v} R_v(z, E_e)^2 \, dz \#(31)$$

$$V_{cell}(E_e) = \pi \, R(E_e)^2 \, 2H(E_e) \#(32)$$

Thus, porosity evolution might be registered as $f(E_e) = V_{void}(E_e)/V_{cell}(E_e)$. This third approach is followed in the present work and the procedure is automatized using a python script integrated in ABAQUS.

Whereas porosity evolution might be an indicator of the damage process, the change in void shape during loading also depends on the failure mechanisms and the triaxiality parameter so the variable $W = H_v/R_v$ is also registered at each strain E_e.

In order to evaluate the failure mechanism, a quantitative criterion must be established for the discrimination between shearing and necking modes of void coalescence:

- **Shearing failure**: the localisation of plastic instabilities in a shear band is translated to a new criterion determined by an increase in the plastic strain rate in a narrow band whereas the deformation outside the band does not increase, i.e. $\dot{\varepsilon}^p_{band}/\dot{\varepsilon}^p_{bulk} \to \infty$. More details can be found in [15].
- **Necking failure**: when $dE_r/dt \to 0$ it is assumed that plasticity is localised in the ligament so necking is happening [13]. It is equivalent to the condition of constant radial displacement of the unit cell $dU_r/dt \to 0$.

Numerical instabilities are usually found when the shearing failures occur due to the very high $\dot{\varepsilon}^p_{band}$. Due to the extremely fast creation of traps and hydrogen depletion of lattice sites, diffusion analysis is also unstable after shearing failure. Thus, post-shearing necking cannot be always modelled even though there is very unlikely to happen in a real void. Sometimes, the shearing criterion is not so clear and, even though a shear band might be defined, the peak of the ratio $\dot{\varepsilon}^p_{band}/\dot{\varepsilon}^p_{bulk}$ is less than 10. In those cases, both shearing and the subsequent necking failure are analysed. The present simulations consider an axisymmetric model but initially the void is spherical and the elastic-plastic material response is considered as isotropic. However, Benzerga et al. [59] have recently found that anisotropic effects, i.e. void shape influence and anisotropic plasticity or texture effects, might trigger shear failure. Thus, shearing failures could happen before significant softening is promoted by local hydrogen accumulation. The implications of this grain-size anisotropy in the hydrogen-enhanced shear localisation is out of the scope of the present paper but it should be better understood in future.

5.1. Triaxiality influence without hydrogen

In the absence of hydrogen, the void unit cell defined in Table 2 and 3 is simulated with a very slow loading ($\dot{U}_z$ = 10^{-3} mm·s^{-1}). As already said, without transient effects and a negligible strain rate hardening, the unit cell dimensions are trivial. As expected in the uncharged situation, i.e. without hydrogen-enhanced softening, a necking failure is obtained when $dU_r/dt \to 0$. The

end of lateral deformation might be appreciated in Figure 7; the higher triaxiality is applied, the lower equivalent strain is reached at failure. The deformed cells included in Figure 7 are not to scale but they show how the low triaxiality η = 0.7, which might be found in the absence of stress concentrators, produces a significant elongation of the void and generalised plastic strain.

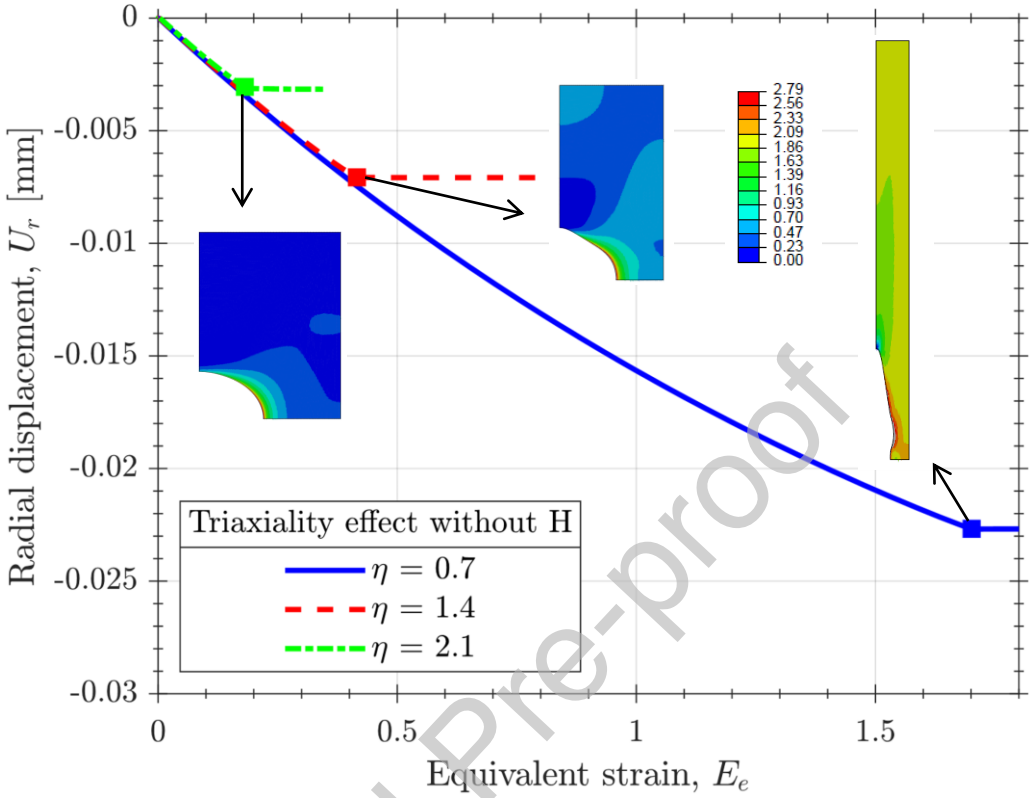

Figure 7. Radial displacement evolution of the exterior lateral face of the unit cell subjected to different triaxiality values. Necking failure criterion is extracted from this plot. The deformed cells at necking are not to scale and colours indicate local equivalent plastic strain.

Porosity evolution and void shapes are also registered and plotted in Figure 8. The necking failures observed in Figure 7, i.e. stabilisation of the radial cell deformation, are indicated for the corresponding equivalent strain. The critical porosity is higher for a low triaxiality, but it must be noted that for high triaxialities the void grows in both axial and radial direction so the void shape factor W is nearly 1 (as for η = 1.4) or it even might decrease (as for η = 2.1). The smooth evolution of the void shape has an abrupt change, especially for the lowest triaxiality value, in the necking failure point, as shown in Figure 9. For η = 0.7, the ligament and the void surface are very distorted, as shown in deformed cells in Figure 7, and when necking occurs, the axial void radius, i.e. R_v, decreases whereas H_v is still increasing at a very high rate, leading to an abrupt change in void aspect ratio.

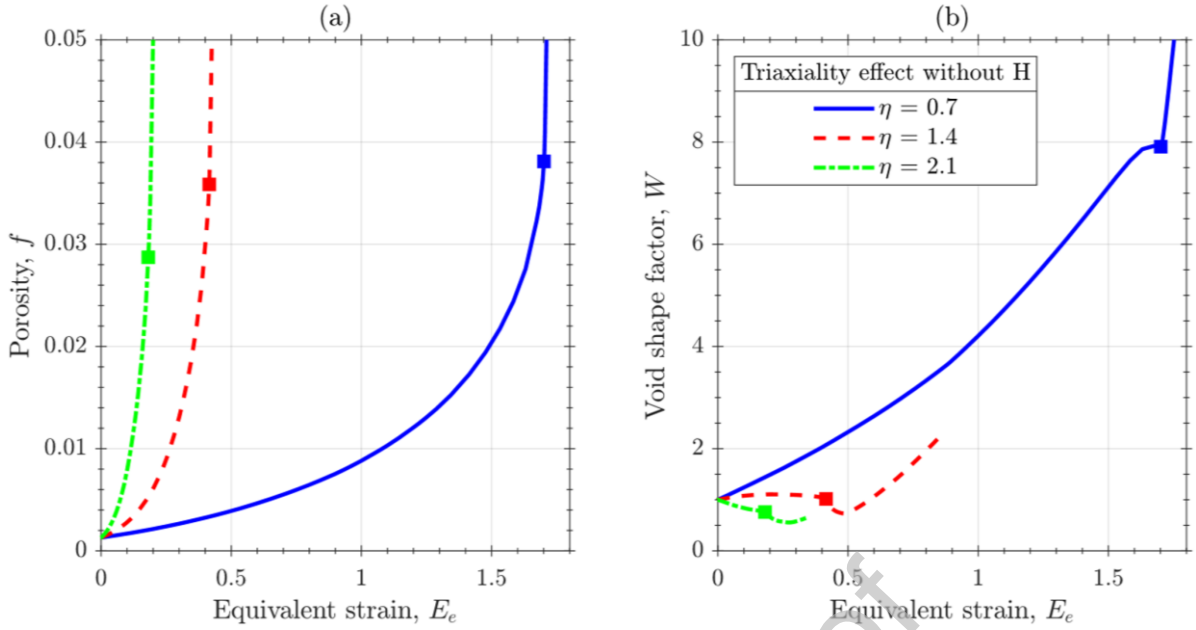

Figure 8. (a) Porosity evolution and (b) evolution of void shape factor ($W = H_v/R_v$) for different triaxialities.

A critical porosity of 0.038 and a final equivalent strain of 1.71 are obtained for η = 0.7. Those values are hard to be found in reality because when the first voids coalesce, and a crack starts to propagate, so the local triaxiality increases even in a tensile test without initial notches. Nevertheless, it is problematic to model the ductile mechanism of failure in a hydrogen environment at high triaxialities; in these cases, the competition and/or synergy between localised plasticity and decohesion must be clarified. The present study is limited to the study of void growth and the subsequent ductile failure; hence the following sections are focused on low triaxialities: η = 0.7.

5.2. Hydrogen redistribution without softening

Before simulating hydrogen-enhanced local softening, redistribution along the deforming cell has been studied with the aim of assessing the effect of strain rate in trapping phenomena. Two transport mechanisms are critical for the distribution of hydrogen between trapping and lattice sites: (i) kinetic exchange governed by McNabb and Foster equations [31] and (ii) fast creation of traps and the modification of the mass balance proposed by Krom et al. [10]. However, Krom et al. state that even at high strain rates, Oriani's thermodynamic equilibrium might be assumed since the frequency of hop attempts for the hydrogen atom is extremely high, in this case, the Debye frequency $\nu = 10^{13}$ s^{-1} [32].

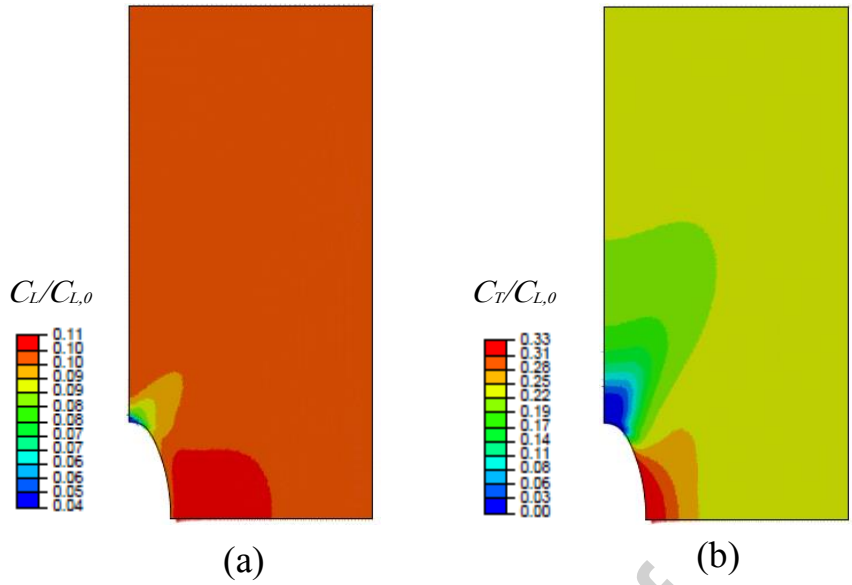

Figure 10. Hydrogen concentrations at lattice and trapping sites at E_e = 0.5, for E_b = 40 kJ/mol, $C_{L,0}$ = 10^{-3} wt ppm and $\dot{U}_z$ = 10 mm/s.

Figure 10 shows the distribution of hydrogen in an insulated cell long before (E_e = 0.5) the necking failure (E_e = 1.71). As expected, lattice hydrogen peak is located at the hydrostatic stress maximum, i.e. at a certain distance from the void in the radial plane of symmetry, whereas the trapped hydrogen accumulates near the void surface where the plastic strain is maximum. At higher values of E_e, plastic strain is spread over the whole cell and some plastic instabilities are triggered (necking or shearing mechanisms) so the distribution of hydrogen is less predictable. Figure 11 shows the comparison between concentrations at E_e = 0.5 and those at E_e = 1.0 in both radial and axial directions, as indicated in the scheme. Diffusion times elapsed for $\dot{U}_z$ = 10 mm/s at the analysed equivalent strains, i.e. E_e = 0.5 and E_e = 1.0, are 0.05 mm and 0.10 seconds, approximately.

Additionally, a critical influence of initial concentration is found even though concentrations are normalised. As shown in Figure 11, at $C_{L,0}$ = 1 wt ppm the trapping effect is very slight; on the contrary, for a lower initial concentration, $C_{L,0}$ = 10^{-3} wt ppm, and bearing in mind that the displacement rate is so high that equilibrium is not reached, traps attract hydrogen while lattice sites are depleted. This void behaviour is similar to the results found by Krom et al. [10] for hydrogen transport near an insulated crack tip during fast loads. In that case, the effect of the strain rate on lattice hydrogen depletion is less critical as C_L increases [10].

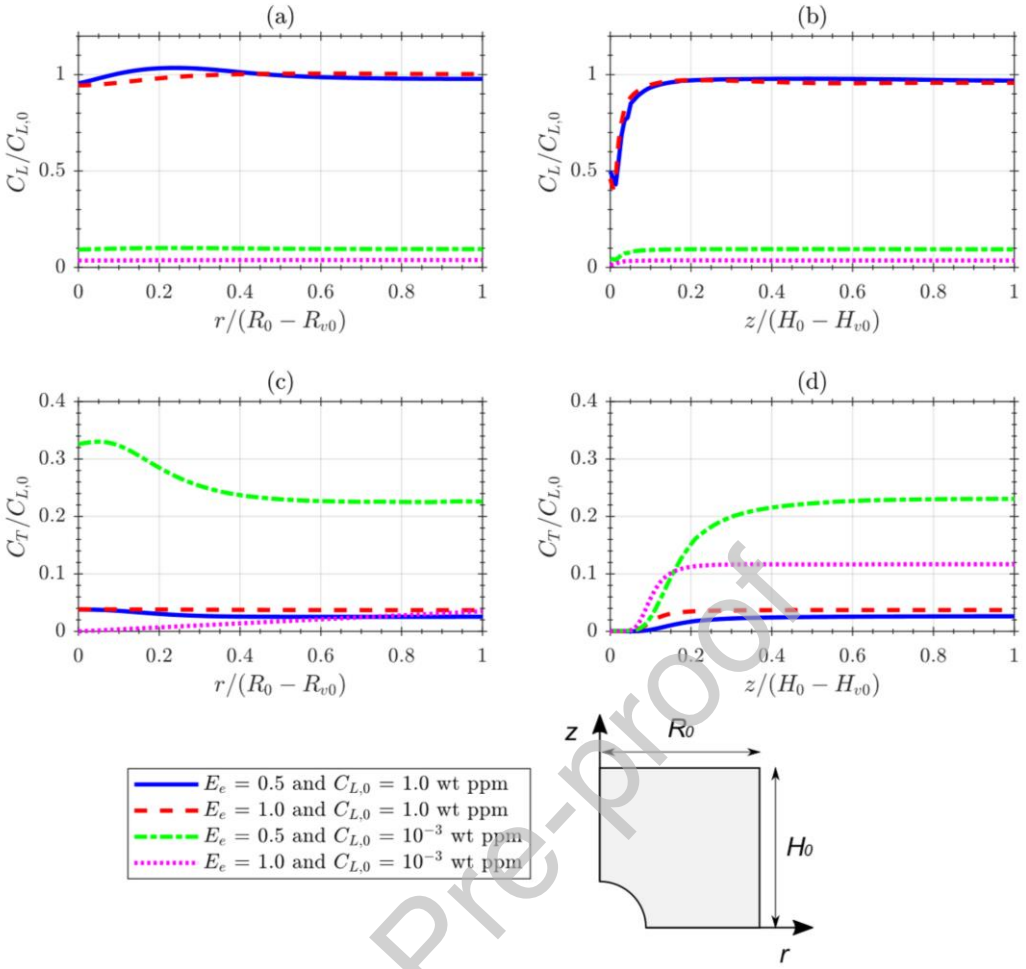

Figure 11. Hydrogen concentrations at lattice and trapping sites in radial and axial symmetry planes for $\dot{U}_z$ = 10 mm/s.

It must be recalled that hydrogen distributions tend to the equilibrium configuration, as might be deduced by the semi-analytic solution [57] implemented to solve McNabb and Foster's equations. Even though only E_b = 40 kJ/mol is evaluated in the present study, the process of trap saturation and the effect of initial lattice concentration will depend on the binding energy, as illustrated in Figure 12. The trap capacity to deplete lattice sites will change during loading since trap density increases with plastic strain. Thus, the balance between C_L and the asymptotic C_T that would be found at equilibrium is relative to the trap energy and density; the dependency of N_T on ε^p is here assumed to follow equation (2).

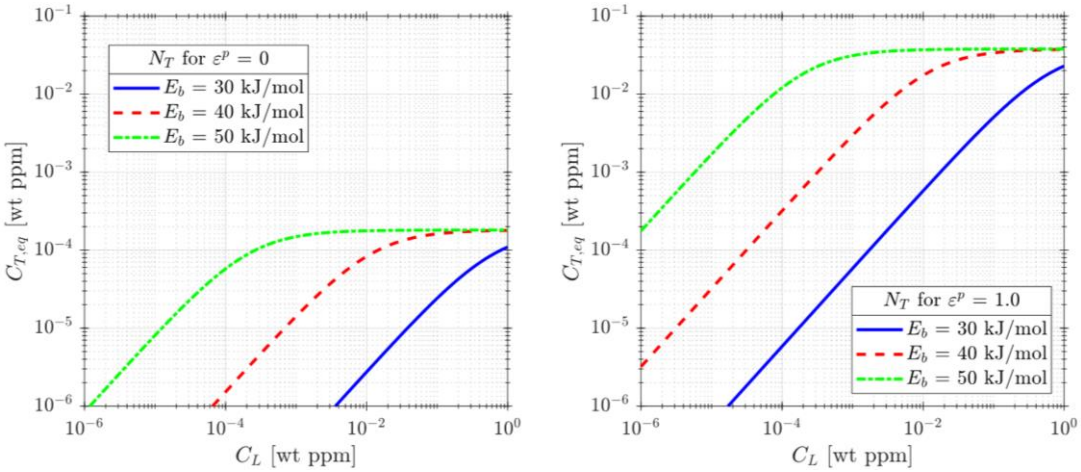

Figure 12. Relationship between hydrogen concentrations at lattice and the corresponding equilibrium concentration at trapping sites for different binding energies and for two level of trap densities N_T: for ε^p = 0 (left), and for on ε^p = 1 (right).

With the aim of quantifying the strain rate effect on hydrogen redistribution around the void and the possible influence on local softening and the subsequent ductile mechanism, three displacement rates are simulated in an insulated unit cell, i.e. reproducing short load times in which hydrogen is not able to move from one cell to the neighbour, and compared with the equilibrium situation, i.e. a steady state in which the cell is not insulated and the lattice and trapping sites allocate as much hydrogen as it is required. In the latter situation, hydrogen should be absorbed from the exterior environment or from other material regions that are subjected to a lower stress state; hence the equilibrium case is always more detrimental for hydrogen-enhanced softening. However, as shown for the softening law h_2 in Figure 2, when the threshold is achieved at high concentrations, a subsequent hydrogen accumulation does not influence softening.

Figure 13 plots hydrogen concentrations along the radial direction at the beginning of the load (E_e = 0.3) for $\dot{U}_z$ equal to 1, 100 and 10^4 mm/s. Even though these three insulated simulations result in a lower hydrogen accumulation in comparison with the equilibrium condition, it can be concluded that there is a strain rate effect due to the depletion of lattice sites during fast creation of traps. At $\dot{U}_z$ = 1 mm/s, the concentration profiles show a shape similar to the equilibrium results: a C_L peak is observed due to hydrostatic stress and C_T raises in the void surface due to equivalent plastic strain. However, this curve shape changes for higher displacement rates and for $\dot{U}_z$ = 10^4 mm/s the lattice sites are almost empty.

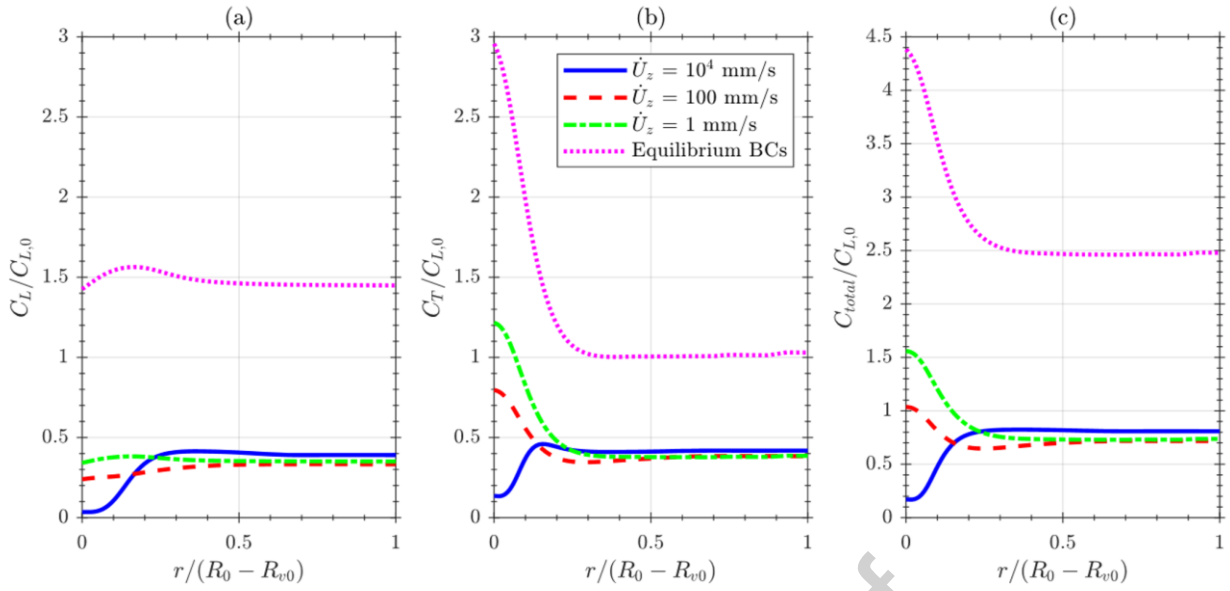

Figure 13. Hydrogen concentrations in (a) lattice sites, (b) trapping sites and (c) total concentration. Results calculated at the radial symmetry plane for E_e = 0.3, E_b = 40 kJ/mol, $C_{L,0}$ = 10^{-3} wt ppm and different strain rates.

Effective diffusion coefficient has been calculated at each point for the unit cell using the local concentrations and following equation (12). The ratio D_{eff}/D_L has been plotted Figure 14.(a) along the radial symmetry plane. It can be seen how the depletion of hydrogen for very high strain rates is related to a higher effective diffusivity near the void. Additionally, the diffusion length x_{diff} has been found through expression (11) and plotted in Figure 14.(b). Strain rate $\dot{E}_e$ was determined as the equivalent strain increment ΔE_e divided by the time increment within the MPC subroutine. For high strain rates the diffusion length scale is lower than the cell dimensions $x_{diff} < R_0$ whereas for $\dot{U}_z$ = 1 mm/s the diffusion length scale is greater than the cell initial radius. However, here the effective diffusivity value is useful just as an indicator of transport delay due to trapping but its expression assumes equilibrium and neglects Krom's term influence, so the x_{diff} value must be only considered qualitatively.

The observed transient effects invalidate the quasi-static assumption and the importance of length scales, cell boundary conditions and strain rate influence must be considered. However, the insulated assumption might be controversial for intermediate load rates and multi-scale strategies must be used to simulate a global model enriched with void constitutive behaviour.

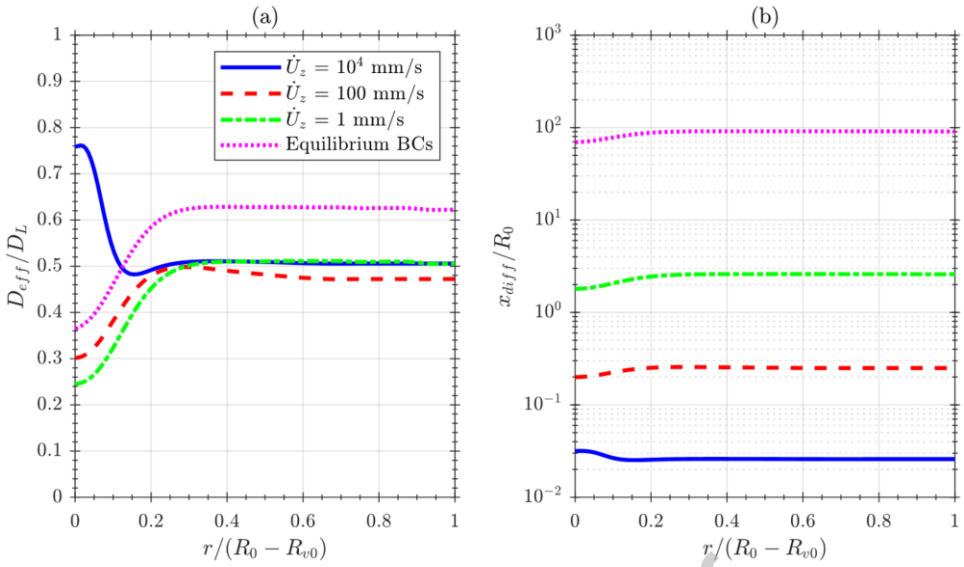

Figure 14. Strain rate effect on (a) effective diffusivity, and (b) diffusion length scale. Results calculated at the radial symmetry plane for E_e = 0.3, E_b = 40 kJ/mol, $C_{L,0}$ = 10^{-3} wt ppm and different strain rates.

5.3. Hydrogen softening effect

After observing that hydrogen concentration is dependent on the loading rate, the void growth and the final stage of failure due to plastic instabilities are analysed. For that purpose, the three softening laws plotted in Figure 2 are implemented as a function of local concentration: linear softening and sigmoidal softening with two different k values. Therefore, a less pronounced hydrogen effect is expected for $\dot{U}_z$ = 10^4 mm/s from the results shown in Figure 13 since a region near the void is depleted of hydrogen. Figure 15 confirms this hypothesis as porosity evolution is very insensitive to hydrogen effects during the cell loading process; however, the failure strain and the critical porosity values are reduced because of hydrogen. The linear law and the sigmoidal softening with k = 5 show very similar behaviour whereas for k = 15 necking occurs earlier. Figure 14 also shows the void shape evolution and it is demonstrated that even though porosity evolution does not change before ductile failure, the axial growth of void starts to be limited after E_e = 1.0 so the void shape factor W reaches a plateau due to the early beginning of necking. It must be noted that the E_e axis in Figure 15.(a) and (b) does not start at zero since the first stage of void growth is unaltered.

The same evaluation is performed for a lower displacement rate, $\dot{U}_z$ = 1 mm/s, but still with insulated cell conditions and shown in Figure 16. Now, a critical hydrogen effect is observed for all the softening laws at very low equivalent strains. The most detrimental softening behaviour is the sigmoidal with k = 15, while the linear softening shows a more stable void growth. Nevertheless, the early failures indicate a possible change of mechanism from necking to shearing mode.

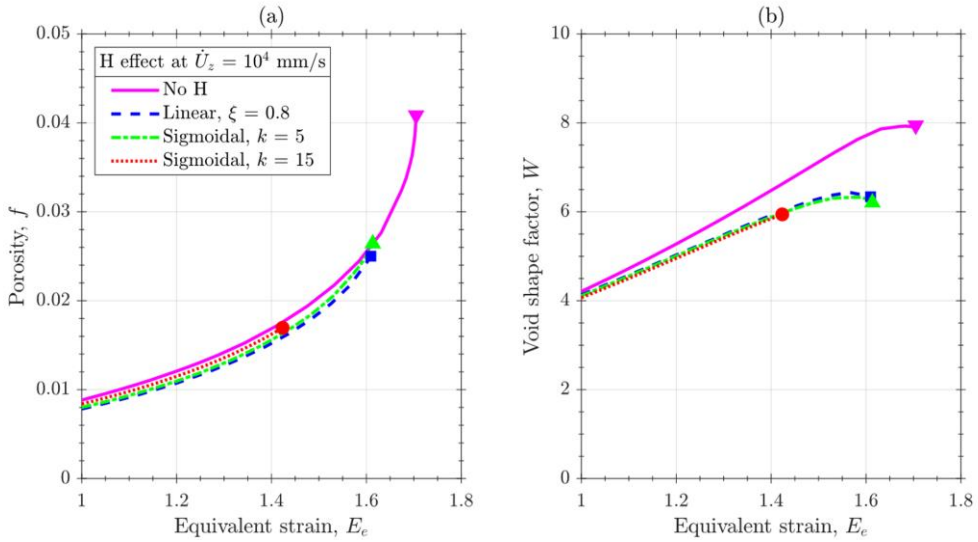

Figure 15. Hydrogen softening effect in (a) porosity evolution, (b) void shape evolution for E_b = 40 kJ/mol, $C_{L,0}$ = 10^{-3} wt ppm and strain rate $\dot{U}_z$ = 10^4 mm/s.

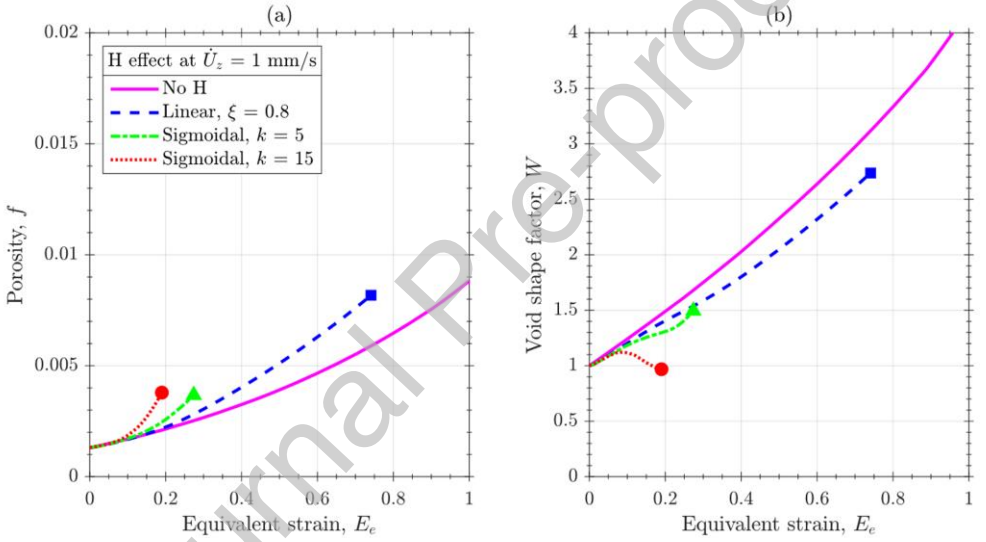

Figure 16. Hydrogen softening effect in (a) porosity evolution, (b) void shape evolution for E_b = 40 kJ/mol, $C_{L,0}$ = 10^{-3} wt ppm and strain rate $\dot{U}_z$ = 1 mm/s.

The void deformed geometry and the contours of equivalent plastic strain are represented in Figure 17. Two facts are deduced from this:

(i) a shear band is formed for sigmoidal softening, especially for k = 15 because there is a very steep reduction of the local yield stress, as shown in Figure 2. The shearing failure at very low strains might be regarded macroscopically as embrittlement even though the triggering mechanism is an enhanced localised plasticity.

(ii) linear softening does not produce shear banding, but the necking is produced at very low strains. The mechanism still remains the same but this also might be associated with macroscopic embrittlement.

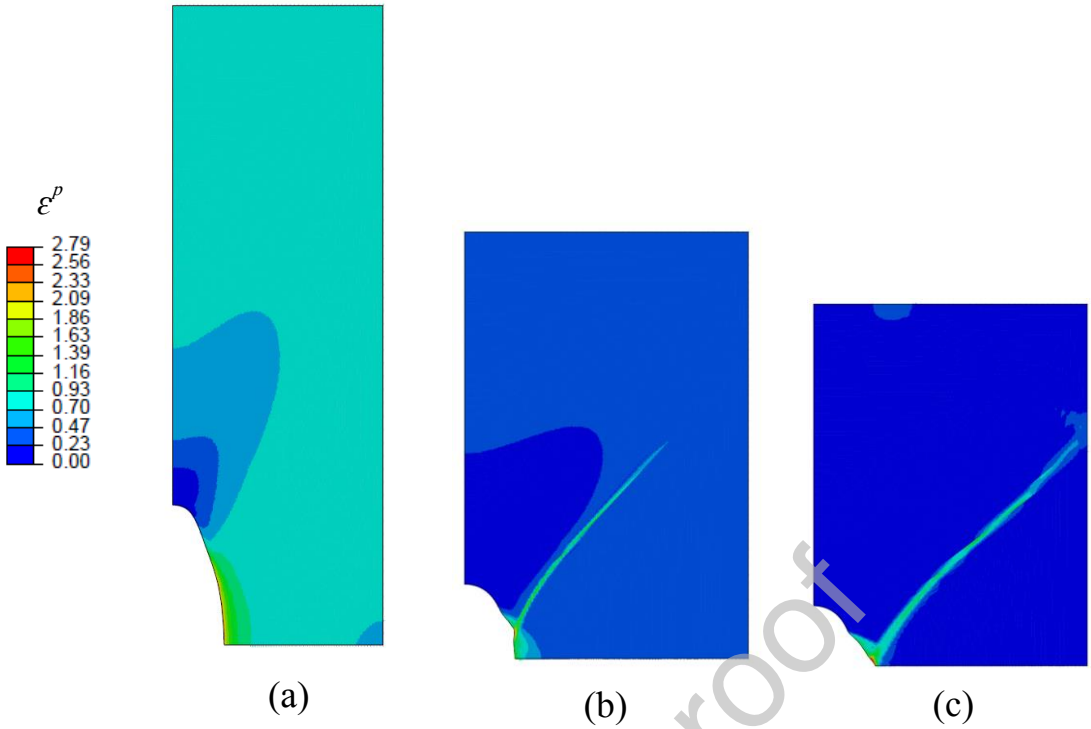

Figure 17. Void failures in (a) linear softening with ξ = 0.8, (b) sigmoidal softening with k = 5, (c) sigmoidal softening with k = 15, for E_b = 40 kJ/mol, $C_{L,0}$ = 10^{-3} wt ppm and strain rate $\dot{U}_z$ = 1 mm/s.

In these FE simulations, the W shape is a good indicator of the failure mechanism: when the shear band appears, the void radius R_v grows due to the plastic instability while its axial radius H_v grows very slow. This irregular evolution of W at very low triaxialities is and indicator of shear band formation. It must be noted that in the present paper, the loading inputs are the axial displacement rate $\dot{U}_z$ and the constant triaxiality η; however, "strain rate" effects have been discussed for consistency with the literature. Due to the different material response at different displacement rates, when hydrogen or strain rate hardening effects are included, the same $\dot{U}_z$ does not imply the same equivalent strain rate $\dot{E}_e$. This small deviation caused by a strongly coupled material behaviour is not discussed here.

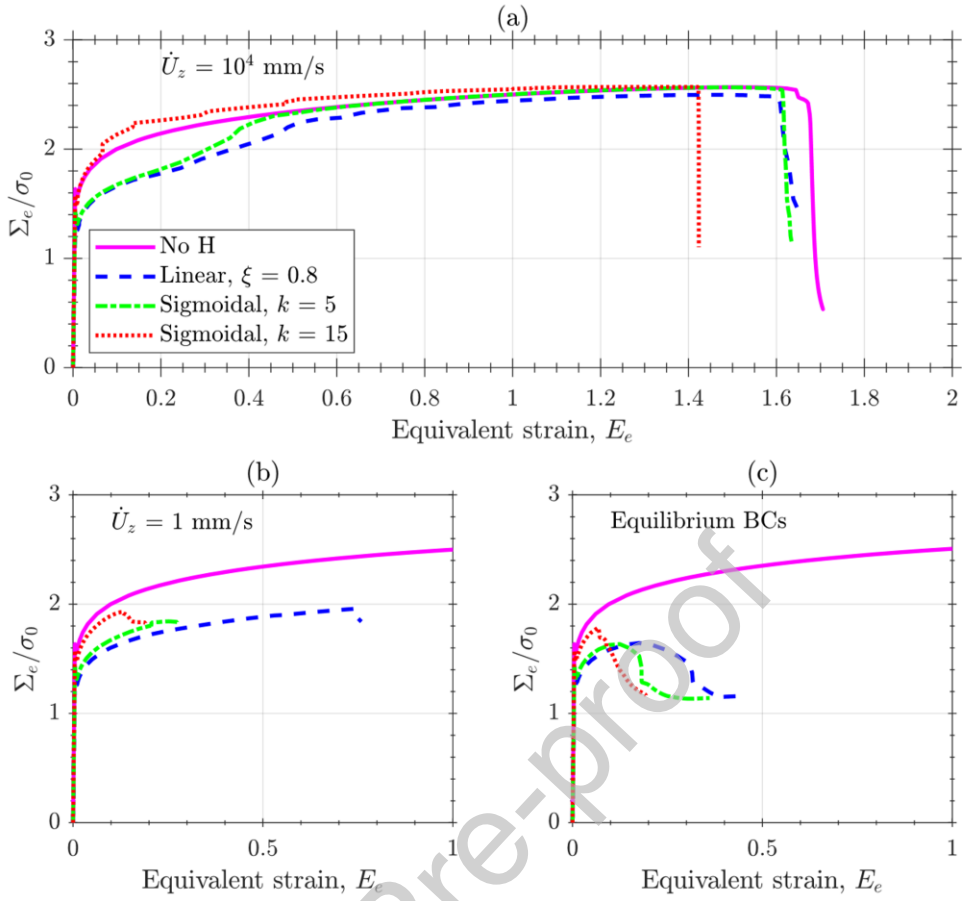

Figure 18. Hydrogen softening effect in the mesoscopic stress-strain response for E_b = 40 kJ/mol, $C_{L,0}$ = 10^{-3} wt ppm and different strain rates: (a) $\dot{U}_z$ = 10^4 mm/s, (b) $\dot{U}_z$ = 1 mm/s and (c) equilibrium boundary conditions.

The stress-strain curve associated with each simulation is obtained by averaging node forces in the cell boundaries and considering the current section; Figure 18 shows equivalent stress versus equivalent strains (Σ_e-E_e) for three different situations: (a) $\dot{U}_z$ = 10^4 mm/s, (b) $\dot{U}_z$ = 1 mm/s and (c) equilibrium boundary conditions and confirms the conclusions observed in Figures 15, 16 and 17. For very fast loads, necking is observed even in the presence of hydrogen. However, the drop in load bearing capacity is observed at lower equivalent strains for the hydrogen-charged cells. As observed in Figure 15, the most critical softening behaviour is found for the sigmoidal law with k = 15, whereas k = 5 results in a material response similar to that obtained with a linear law and ξ = 0.8. For the intermediate situation, necking is observed for the linear law even though the cell suffers a significant mesoscopic softening. On the other hand, sigmoidal softening with k = 15 shows clearly a shearing failure with a drop in equivalent stress at a very low equivalent strain. For the equilibrium condition, i.e. considering thermodynamic equilibrium and neglecting transient effects in hydrogen accumulation, hydrogen promotes shearing regardless the considered softening law. After the stress drop due to the formation of a high strain shear band ($\dot{\varepsilon}^p_{band}/\dot{\varepsilon}^p_{bulk} \to \infty$) a post-shearing plateau is observed. However, simulations are very unstable due to the fast creation of dislocations within this band; the very high plastic strain rate acts as an unrealistically strong sink for hydrogen and

convergence is hard to achieve up to final necking. More details of the post-shearing failure due to necking might be found in [15].

5.4. Strain rate hardening effect

The simulations with $\dot{U}_z$ = 1 mm/s have shown a very strong hydrogen effect and the corresponding embrittlement due to shearing or early necking. However, for the sake of simplicity, results from previous sections do not include a strain rate hardening effect. The possibility that strain rate hardening overcomes the hydrogen-enhanced softening at certain conditions and might supress shear band formation is evaluated now. For that purpose, the function h_3 from equation (18) is included in the whole hardening law h, with $\dot{\varepsilon}_0^p$ = 0.001 s^{-1} and two sensitivity exponents: m = 0.05 and m = 0.10. The value m = 0 indicates no strain rate hardening, i.e. h_3 = 1.

Figure 19 shows that strain rate hardening produces a failure at higher equivalent strains and, for the stronger hardening, m = 0.10 at a higher critical porosity. The void shape change is also higher when strain rate hardening is included. This might be seen as a counterbalance of hydrogen effects; nevertheless, shearing failure is still found as shown by the void deformed geometries in Figure 20.

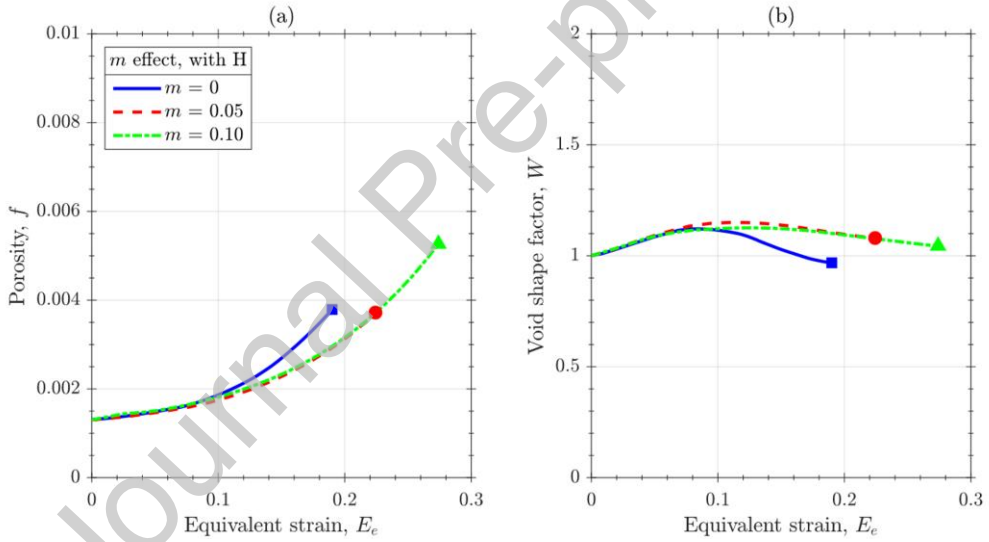

Figure 19. Effect of strain rate sensitivity in (a) porosity evolution, (b) void shape evolution for k = 15, E_b = 40 kJ/mol, $C_{L,0}$ = 10^{-3} wt ppm and strain rate $\dot{U}_z$ = 1 mm/s.

Representing the contour lines of the hardening function, i.e. $h = \sigma_Y/\sigma_0 = h_1 h_2 h_3$, the competition between strain hardening, hydrogen-induced softening and strain rate hardening might be assessed. Regions with $h < 1$ are more susceptible to plastic instabilities because in that places a local softening is occurring. Figure 20 shows that, even though plastic strain is high, for a sigmoidal softening with k = 15 a band of low h has been formed before failure (at E_e = 0.15) and hydrogen is able to trigger the band development. This band formation is not observed when strain rate hardening is included since the hardening law h takes higher values.

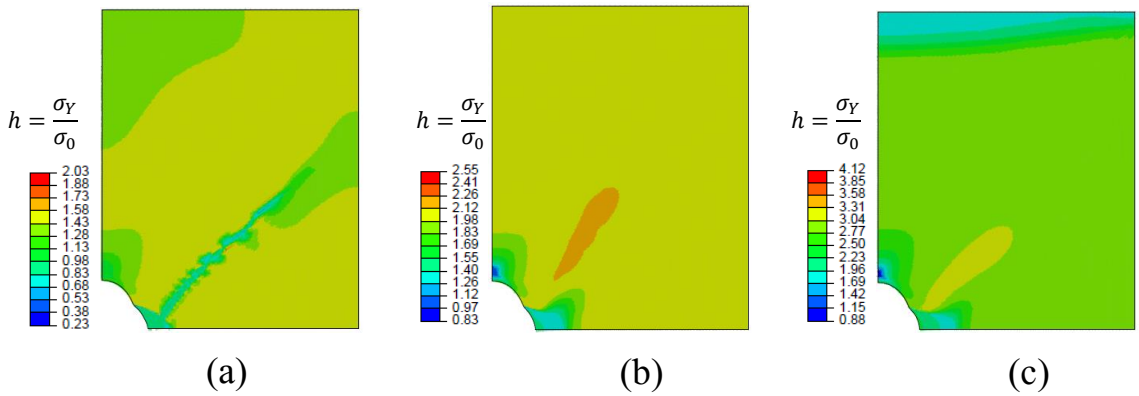

Figure 20. Void geometry and contours of hardening law $h = h_1 h_2 h_3$ at E_e = 0.15: (a) no strain rate hardening, (b) m = 0.05 and (c) m = 0.10; for k = 15, E_b = 40 kJ/mol, $C_{L,0}$ = 10^{-3} wt ppm and strain rate $\dot{U}_z$ = 1 mm/s. The scale limits of h are different for each subfigure.

6. Discussion and concluding remarks

Numerical implementation of a local softening due to hydrogen has been performed in the framework of the HELP theory that states that hydrogen enhances a localised plasticity by increasing dislocation mobility. The implications of this softening have been traditionally evaluated in a quasi-static scenario in which length and time scales are trivial. However, transient effects are due to an intrinsic length scale associated with diffusion and it has been demonstrated that the kinetic consideration of hydrogen redistribution, especially the plastic strain rate term proposed by Krom et al. [10], influences void growth and the final ductile failure.

The presented numerical methodology is only a first step for hydrogen embrittlement mitigation and prognosis since void behaviour should be incorporated in damage models, e.g. Gurson-based [60], cohesive [61], or phase field models [62]. Hydrogen effects on void growth are hard to be validated with empirical results for two main reasons: (i) hydrogen transport parameters are unknown for most materials and the experimental methodology aimed at characterising trapping behaviour is still not consistent -even though permeation and TDS tests are commonly used- so binding energies and trapping densities are hard to be univocally determined. Additionally, softening laws due to local hydrogen concentrations are hypothesised and deduced from some experimental results found from literature [15,63] but they are far from a predictive expression in the hydrogen embrittlement prognosis. Dislocation behaviour in the presence of hydrogen must be better understood for the validation of these results enhanced by a phenomenological local softening; (ii) the numerical strategy presented here has the objective of predicting void behaviour during growth and early coalescence; however, real hydrogen-related failures show a combination of dimpled surfaces and flat facets whereas decohesion promoted by hydrogen is not considered here. Nevertheless, results from literature show some phenomena that our model could evaluate: (i) the observed shift in tensile tests in the presence of hydrogen from a necking mode of failure to a shearing mode [6,7]; (ii) strain-rate effect and the concept of diffusion lengths associated with hydrogen transport towards the fracture process zone [22,25].

The present paper has focused on low triaxialities since in these cases void growth and coalescence are the critical mechanisms whereas hydrogen-enhanced decohesion might be ignored. In the absence of hydrogen, a unit cell subjected to a low triaxiality reaches a very high strain and critical porosity before necking failure (Figures 8 and 9). These phenomena have been studied through Finite Element simulations and an ABAQUS subroutine that keeps a

constant triaxiality and registers the main cell variables: cell displacements, mesoscopic stresses and strains, porosity evolution and void shape factor.

Hydrogen redistribution at low triaxialities have been considered in two scenarios: a quasi-static situation in which hydrogen follows the thermodynamic equilibrium configuration and a fast load condition where the unit cell is analysed in a transient scheme and with insulated boundary conditions since it is assumed that there is not enough time for hydrogen to diffuse from outer regions (Figure 6). Four transient effects are considered here. All these phenomena are influenced by the loading time, i.e. by the strain rate; (i) transient diffusion, governed by diffusivity and by the cell size; (ii) kinetic exchange between traps and lattice sites, governed by the McNabb and Foster equations; (iii) fast creation of traps, governed by Krom's term; and (iv) strain rate hardening, governed by the sensitivity exponent m. This complex coupled scheme has been evaluated step by step. First, hydrogen redistribution without softening has been simulated. It has been found that hydrogen is depleted from regions near the void surface at very high displacement rates (Figure 13). However, these phenomena strongly depend on the trap features, i.e. on binding energy and trap density, as well as on the initial hydrogen concentration (Figures 11 and 12). It also has been demonstrated that this transient dependency of hydrogen transport critically determines the void failure when hydrogen-induced softening is implemented (Figures 15 and 16). Finally, it has been demonstrated how strain rate hardening might delay the shear band formation.

Hydrogen local softening has been modelled here through phenomenological laws that should be empirically contrasted and also fed by atomistic and/or dislocation dynamics simulations. It must be also emphasised that the initially uniform concentration within the void unit cell is a critical value: only for a low initial lattice concentration the strain rate influence in the transport phenomena is observed. Additionally, the assumption that initial hydrogen concentration in lattice sites represents the softening threshold concentration, i.e. that $C_{L,0} = C_0^s$, is an oversimplification. Despite these limitations within the continuum modelling framework of localised plasticity promoted by hydrogen, a robust scheme for the implementation of coupled hydrogen diffusion and softening has been presented in the present paper. The quasi-static oversimplifications have been solved through a transient analysis in which the strain rate influence on hydrogen redistribution and the competition between softening and hardening phenomena have been evaluated.

ACKNOWLEDGEMENTS

The authors gratefully acknowledge financial support from the project MINECO Refs: MAT2014-58738-C3-2-R and RTI2018-096070-B-C33. A. Díaz wishes to thank the Nanomechanical Lab of NTNU for providing hospitality during his research stay and also acknowledges the pre-doctoral mobility grant funded by University of Burgos (UBU 2016: 12MA-461AA-487.01). Z. Zhang would like to thank the Research Council of Norway for the support via the M-HEAT (294689) and HyLine project.

REFERENCES

[1] H.K. Birnbaum, P. Sofronis, Hydrogen-enhanced localized plasticity—a mechanism for hydrogen-related fracture, Mater. Sci. Eng. A. 176 (1994) 191–202. doi:http://dx.doi.org/10.1016/0921-5093(94)90975-X.

[2] P. Sofronis, H.K. Birnbaum, Mechanics of the hydrogendashdislocationdashimpurity interactions—I. Increasing shear modulus, J. Mech. Phys. Solids. 43 (1995) 49–90. doi:http://dx.doi.org/10.1016/0022-5096(94)00056-B.
[3] P. Sofronis, Y. Liang, N. Aravas, Hydrogen induced shear localization of the plastic flow in metals and alloys, Eur. J. Mech. - A/Solids. 20 (2001) 857–872. doi:http://dx.doi.org/10.1016/S0997-7538(01)01179-2.
[4] M.L. Martin, M. Dadfarnia, A. Nagao, S. Wang, P. Sofronis, Enumeration of the hydrogen-enhanced localized plasticity mechanism for hydrogen embrittlement in structural materials, Acta Mater. 165 (2019) 734–750. doi:10.1016/J.ACTAMAT.2018.12.014.
[5] S.P. Lynch, Progress towards understanding mechanisms of hydrogen embrittlement and stress corrosion cracking, in: Corros. 2007, NACE International, 2007.
[6] T. Matsuo, Effect of hydrogen and prestrain on tensile properties of carbon steel SGP (0.078 C-0.012 Si-0.35 Mn, mass%) for 0.1 MPa hydrogen pipelines, Trans. Japan Soc. Mech. Eng. Ser. A. 74 (2008) 120–129.
[7] T. Matsuo, J. Yamabe, S. Matsuoka, Effects of hydrogen on tensile properties and fracture surface morphologies of Type 316L stainless steel, Int. J. Hydrogen Energy. 39 (2014) 3542–3551. doi:10.1016/J.IJHYDENE.2013.12.099.
[8] C.D. Beachem, A new model for hydrogen-assisted cracking (hydrogen "embrittlement"), Metall. Trans. 3 (1972) 441–455.
[9] P. Sofronis, R.M. McMeeking, Numerical analysis of hydrogen transport near a blunting crack tip, J. Mech. Phys. Solids. 37 (1989) 317–350. doi:http://dx.doi.org/10.1016/0022-5096(89)90002-1.
[10] A.H.M. Krom, R.W.J. Koers, A. Bakker, Hydrogen transport near a blunting crack tip, J. Mech. Phys. Solids. 47 (1999) 971–992.
[11] E. Martínez-Pañeda, S. del Busto, C.F. Niordson, C. Betegón, Strain gradient plasticity modeling of hydrogen diffusion to the crack tip, Int. J. Hydrogen Energy. 41 (2016) 10265–10274. doi:https://doi.org/10.1016/j.ijhydene.2016.05.014.
[12] Z.. Zhang, C. Thaulow, J. Ødegård, A complete Gurson model approach for ductile fracture, Eng. Fract. Mech. 67 (2000) 155–168. doi:10.1016/S0013-7944(00)00055-2.
[13] A.A. Benzerga, J.-B. Leblond, Ductile Fracture by Void Growth to Coalescence, Adv. Appl. Mech. 44 (2010) 169–305. doi:10.1016/S0065-2156(10)44003-X.
[14] D.C. Ahn, P. Sofronis, R. Dodds, Modeling of hydrogen-assisted ductile crack propagation in metals and alloys, Int. J. Fract. 145 (2007) 135–157. doi:10.1007/s10704-007-9112-3.
[15] H. Yu, J.S. Olsen, J. He, Z. Zhang, Hydrogen-microvoid interactions at continuum scale, Int. J. Hydrogen Energy. 43 (2018) 10104–10128. doi:10.1016/J.IJHYDENE.2018.04.064.
[16] N.A. Fleck, J.W. Hutchinson, A phenomenological theory for strain gradient effects in plasticity, J. Mech. Phys. Solids. 41 (1993) 1825–1857. doi:http://dx.doi.org/10.1016/0022-5096(93)90072-N.
[17] E. Martínez-Pañeda, C.F. Niordson, On fracture in finite strain gradient plasticity, Int. J. Plast. 80 (2016) 154–167. doi:https://doi.org/10.1016/j.ijplas.2015.09.009.
[18] M.F. Horstemeyer, M.I. Baskes, S.J. Plimpton, Length scale and time scale effects on the plastic flow of fcc metals, Acta Mater. 49 (2001) 4363–4374. doi:10.1016/S1359-6454(01)00149-5.
[19] L. Fokoua, S. Conti, M. Ortiz, Optimal Scaling in Solids Undergoing Ductile Fracture by Void Sheet Formation, Arch. Ration. Mech. Anal. 212 (2014) 331–357. doi:10.1007/s00205-013-0687-8.
[20] X.Q. Wu, I.S. Kim, Effects of strain rate and temperature on tensile behavior of hydrogen-charged SA508 Cl.3 pressure vessel steel, Mater. Sci. Eng. A. 348 (2003) 309–318. doi:10.1016/S0921-5093(02)00737-2.
[21] S. Matsuoka, H. Tanaka, N. Homma, Y. Murakami, Influence of hydrogen and frequency on fatigue crack growth behavior of Cr-Mo steel, Int. J. Fract. 168 (2011) 101–112. doi:10.1007/s10704-010-9560-z.

[22] L.B. Peral, A. Zafra, S. Blasón, C. Rodríguez, J. Belzunce, Effect of hydrogen on the fatigue crack growth rate of quenched and tempered CrMo and CrMoV steels, Int. J. Fatigue. 120 (2019) 201–214. doi:10.1016/J.IJFATIGUE.2018.11.015.
[23] T. Depover, F. Vercruysse, A. Elmahdy, P. Verleysen, K. Verbeken, Interpretation of the hydrogen effect on the static and dynamic tensile behaviour of dual phase steel, in: Proc. Third Int. Conf. Met. Hydrog., 2018: pp. 1–14.
[24] A. Zafra, L.B. Peral, J. Belzunce, C. Rodríguez, Effect of hydrogen on the tensile properties of 42CrMo4 steel quenched and tempered at different temperatures, Int. J. Hydrogen Energy. 43 (2018) 9068–9082. doi:10.1016/J.IJHYDENE.2018.03.158.
[25] L.B. Peral, A. Zafra, J. Belzunce, C. Rodríguez, Effects of hydrogen on the fracture toughness of CrMo and CrMoV steels quenched and tempered at different temperatures, Int. J. Hydrogen Energy. 44 (2019) 3953–3965. doi:10.1016/J.IJHYDENE.2018.12.084.
[26] H. Feng, M.. Bassim, Finite element modeling of the formation of adiabatic shear bands in AISI 4340 steel, Mater. Sci. Eng. A. 266 (1999) 255–260. doi:10.1016/S0921-5093(99)00026-X.
[27] Z.G. Zhu, R.C. Batra, Shear band development in a thermally softening viscoplastic body, Comput. Struct. 39 (1991) 459–472. doi:10.1016/0045-7949(91)90054-P.
[28] A.G. McLellan, Non-Hydrostatic Thermodynamics of Chemical Systems, 1970. doi:10.1098/rspa.1970.0017.
[29] A.J. Kumnick, H.H. Johnson, Deep trapping states for hydrogen in deformed iron, Acta Metall. 28 (1980) 33–39. doi:http://dx.doi.org/10.1016/0001-6160(80)90038-3.
[30] R.A. Oriani, The diffusion and trapping of hydrogen in steel, Acta Metall. 18 (1970) 147–157. doi:http://dx.doi.org/10.1016/0001-6160(70)90078-7.
[31] A. McNabb, P.K. Foster, A new analysis of the diffusion of hydrogen in iron and ferritic steels, Trans. Metall. Soc. AIME. 227 (1963) 618–627. doi:citeulike-article-id:4956272.
[32] A.M. Krom, A. Bakker, Hydrogen trapping models in steel, Metall. Mater. Trans. B. 31 (2000) 1475–1482. doi:10.1007/s11663-000-0032-0.
[33] R.B. Bird, W.E. Stewart, E.N. Lightfoot, Transport Phenomena, Wiley, 2007. https://books.google.co.uk/books?id=L5FnNlIaGfcC.
[34] C.-S. Oh, Y.-J. Kim, Coupled analysis of hydrogen transport within abaqus, Trans. Korean Soc. Mech. Eng. A. 33 (2009) 600–606.
[35] A. Díaz, J.M. Alegre, I.I. Cuesta, Coupled hydrogen diffusion simulation using a heat transfer analogy, Int. J. Mech. Sci. 115–116 (2016). doi:10.1016/j.ijmecsci.2016.07.020.
[36] O. Barrera, E. Tarleton, H.W. Tang, A.C.F. Cocks, Modelling the coupling between hydrogen diffusion and the mechanical behaviour of metals, Comput. Mater. Sci. 122 (2016) 219–228. doi:10.1016/J.COMMATSCI.2016.05.030.
[37] M.E. Gurtin, E. Fried, L. Anand, The mechanics and thermodynamics of continua, Cambridge University Press, 2010.
[38] C. V Di Leo, L. Anand, Hydrogen in metals: A coupled theory for species diffusion and large elastic–plastic deformations, Int. J. Plast. 43 (2013) 42–69. doi:http://dx.doi.org/10.1016/j.ijplas.2012.11.005.
[39] A. Einstein, On the theory of the Brownian movement, Ann. Phys. 4 (1906) 371–381.
[40] R. Kirchheim, Monte-carlo simulations of interstitial diffusion and trapping—I. One type of traps and dislocations, Acta Metall. 35 (1987) 271–280. doi:http://dx.doi.org/10.1016/0001-6160(87)90235-5.
[41] R. Kirchheim, U. Stolz, Monte-carlo simulations of interstitial diffusion and trapping—II. Amorphous metals, Acta Metall. 35 (1987) 281–291. doi:http://dx.doi.org/10.1016/0001-6160(87)90236-7.
[42] X.Y. Wu, K.T. Ramesh, T.W. Wright, The effects of thermal softening and heat conduction on the dynamic growth of voids, Int. J. Solids Struct. 40 (2003) 4461–4478. doi:10.1016/S0020-7683(03)00214-2.
[43] M. Dadfarnia, P. Sofronis, T. Neeraj, Hydrogen interaction with multiple traps: Can it be used to mitigate embrittlement?, Int. J. Hydrogen Energy. 36 (2011) 10141–10148. doi:https://doi.org/10.1016/j.ijhydene.2011.05.027.
[44] T. Zhang, W.Y. Chu, K.W. Gao, L.J. Qiao, Study of correlation between hydrogen-

induced stress and hydrogen embrittlement, Mater. Sci. Eng. A. 347 (2003) 291–299. doi:10.1016/S0921-5093(02)00600-7.
[45] S. Taketomi, R. Matsumoto, N. Miyazaki, Atomistic simulation of the effects of hydrogen on the mobility of edge dislocation in alpha iron, J. Mater. Sci. 43 (2008) 1166–1169. doi:10.1007/s10853-007-2364-5.
[46] S. Wang, N. Hashimoto, S. Ohnuki, Hydrogen-induced change in core structures of {110}[111] edge and {110}[111] screw dislocations in iron, Sci. Rep. 3 (2013) 2760. https://doi.org/10.1038/srep02760.
[47] Y. Gu, J.A. El-Awady, Quantifying the effect of hydrogen on dislocation dynamics: A three-dimensional discrete dislocation dynamics framework, J. Mech. Phys. Solids. 112 (2018) 491–507. doi:10.1016/J.JMPS.2018.01.006.
[48] H. Yu, A. Cocks, E. Tarleton, Discrete dislocation plasticity HELPs understand hydrogen effects in bcc materials, J. Mech. Phys. Solids. 123 (2019) 41–60. doi:10.1016/J.JMPS.2018.08.020.
[49] C. Tekoğlu, Representative volume element calculations under constant stress triaxiality, Lode parameter, and shear ratio, Int. J. Solids Struct. 51 (2014) 4544–4553. doi:10.1016/J.IJSOLSTR.2014.09.001.
[50] J. Faleskog, X. Gao, C.F. Shih, Cell model for nonlinear fracture analysis – I. Micromechanics calibration, Int. J. Fract. 89 (1998) 355–373. doi:10.1023/A:1007421420901.
[51] Z.L. Zhang, B. Skallerud, Void coalescence with and without prestrain history, Int. J. Damage Mech. 19 (2010) 153–174.
[52] V. Tvergaard, G. Vadillo, Influence of porosity on cavitation instability predictions for elastic–plastic solids, Int. J. Mech. Sci. 49 (2007) 210–216. doi:10.1016/J.IJMECSCI.2006.08.004.
[53] T. Pardoen, J.. Hutchinson, An extended model for void growth and coalescence, J. Mech. Phys. Solids. 48 (2000) 2467–2512. doi:10.1016/S0022-5096(00)00019-3.
[54] C.F. Niordson, Void growth to coalescence in a non-local material, Eur. J. Mech. - A/Solids. 27 (2008) 222–233. doi:10.1016/J.EUROMECHSOL.2007.07.001.
[55] Z. Chen, C. Butcher, Micromechanics modelling of ductile fracture, Springer, 2013.
[56] A. Díaz, J.M. Alegre, I.I. Cuesta, A review on diffusion modelling in hydrogen related failures of metals, Eng. Fail. Anal. 66 (2016). doi:10.1016/j.engfailanal.2016.05.019.
[57] S. Benannoune, Y. Charles, J. Mougenot, M. Gaspérini, Numerical simulation of the transient hydrogen trapping process using an analytical approximation of the McNabb and Foster equation, Int. J. Hydrogen Energy. 43 (2018) 9083–9093. doi:10.1016/J.IJHYDENE.2018.03.179.
[58] H. Yu, J.S. Olsen, J. He, Z. Zhang, Effects of loading path on the fracture loci in a 3D space, Eng. Fract. Mech. 151 (2016) 22–36. doi:10.1016/J.ENGFRACMECH.2015.11.005.
[59] A.A. Benzerga, N. Thomas, J.S. Herrington, Plastic flow anisotropy drives shear fracture, Sci. Rep. 9 (2019) 1425. doi:10.1038/s41598-018-38437-y.
[60] H. Yu, J.S. Olsen, A. Alvaro, L. Qiao, J. He, Z. Zhang, Hydrogen informed Gurson model for hydrogen embrittlement simulation, Eng. Fract. Mech. (2019) 106542. doi:10.1016/J.ENGFRACMECH.2019.106542.
[61] S. del Busto, C. Betegón, E. Martínez-Pañeda, A cohesive zone framework for environmentally assisted fatigue, Eng. Fract. Mech. (n.d.). doi:https://doi.org/10.1016/j.engfracmech.2017.05.021.
[62] E. Martínez-Pañeda, A. Golahmar, C.F. Niordson, A phase field formulation for hydrogen assisted cracking, Comput. Methods Appl. Mech. Eng. 342 (2018) 742–761. doi:10.1016/J.CMA.2018.07.021.
[63] M. Wang, E. Akiyama, K. Tsuzaki, Effect of hydrogen and stress concentration on the notch tensile strength of AISI 4135 steel, Mater. Sci. Eng. A. 398 (2005) 37–46. doi:https://doi.org/10.1016/j.msea.2005.03.008.

Graphical Abstract